PONTIFICIA UNIVERSIDAD CATOLICA DE CHILE
ESCUELA DE INGENIERIA

HORIZONTAL PENDULUM ELECTROMAGNETIC VIBRATION ENERGY HARVESTER WITH TUNABLE NATURAL FREQUENCY: MODELING AND DESIGN

BENJAMÍN ANDRÉS LAGOS BERRÍOS

Thesis submitted to the Office of Research and Graduate Studies in partial fulfillment of the requirements for the Degree of Master of Science in Engineering

Advisor:

LUCIANO EDUARDO CHIANG SANCHEZ

Santiago de Chile, Septiembre, 2015

PONTIFICIA UNIVERSIDAD CATOLICA DE CHILE
ESCUELA DE INGENIERIA

HORIZONTAL PENDULUM ELECTROMAGNETIC VIBRATION ENERGY HARVESTER WITH TUNABLE NATURAL FREQUENCY: MODELING AND DESIGN

BENJAMÍN ANDRÉS LAGOS BERRÍOS

Members of the Committee:

LUCIANO EDUARDO CHIANG SANCHEZ

MIGUEL ATTILIO TORRES TORRITI

JULIO ANDRES OLEGARIO VERGARA AIMONE

RODRIGO CARO DE KARTZOW

HERNAN SANTA MARIA OYANEDEL

Thesis submitted to the Office of Research and Graduate Studies in partial fulfillment of the requirements for the Degree of Master of Science in Engineering

Santiago de Chile, Septiembre, 2015

To God, my Family and Friends. And to my grandfather Roberto, whose curious mind and faith awoke mine.

ACKNOWLEDGMENTS

I would like to thank all the people who contributed in any way to the work described in this thesis. First and foremost, I am grateful to God for the wellbeing and strength he have given to me to complete this process. I feel the most blessed person on earth for having the opportunity to develop my passion and having such caring people around me.

I would like to express my gratitude to my advisor, Dr. Luciano Chiang. For sharing with me the opportunity to get involved in such an interesting and exciting project.

I would also like to thank my committee, for their reviews and insightful comments.

My sincere thanks also go to the members of the Mechatronics division of DICTUC that supported me, especially to Felipe Bravo for his help and vibration data from heavy vehicles.

I also thank the financial support of CONICYT through the FONDEF project N°D10I1069.

I must also acknowledge all the members of the Mechanical Engineering Department, for their constant help and support in all the technical and administrative issues related to this thesis. Particularly, I would like to thank Luis Valdes, for helping me in the construction of the prototype used in this thesis, and Dr.-Ing. Magdalena Walczak for giving me the first insight on research in 2011.

Also I want to express my deepest gratitude to Dr.-Ing. Aldo Cipriano for allowing me to explore another engineering field and making my first academic contribution, in parallel to this thesis.

I also want to thank to Emilio de la Jara, for his constant encouragement and friendship, but mostly for sharing with me his passion for applied engineering and science.

My deepest gratitude to Father José Raad, whose guidance and support accompanied me in the most difficult moments of this path. With his help I have grown personally.

I also want to express my gratitude to my friends, for their patience, affection and, most of all, for accepting me as I am. The moments we shared, the laughs, meetings and lunches at the campus will always have a special place in my heart.

A very special thanks for my girlfriend Romina, for all her guidance, support and love during this process. I learn every day from you.

Finally, I would also like to thank my family, my parents Andrés and Orieta, my brother Cristian and my second mother and nanny, Juana, for the constant support they provided me through this process and my entire life. Without them, nothing of these would have been possible. Unknowingly them forged in me one of my best qualities, the desire to become better every day.

TABLE OF CONTENTS

LIST OF TABLES

LIST OF FIGURES

RESUMEN

En este artículo presentamos la modelación y consideraciones de diseño para el desarrollo de un cosechador de energía vibratoria electromagnético de tipo rotatorio. Una característica importante es que la configuración de este extractor de energía permite que sea fácilmente personalizable y ajustable en un amplio rango de frecuencias de excitación. Este tipo de extractor de energía está diseñado primordialmente para energizar redes de sensores inalámbricos montados en puntos críticos y de difícil acceso en vehículos pesados o en estructuras sujetas a fuertes vibraciones.

Vibraciones lineales en un punto de la estructura vibrante son transformadas en oscilaciones rotacionales, de tal manera que la frecuencia natural del dispositivo depende del momento de inercia más que de la masa de las partes móviles. El momento de inercia a su vez es modificado fácilmente cambiando la posición relativa de una masa acoplada al sistema con respecto al punto de oscilación rotatoria, de forma que la frecuencia natural puede ser ajustada.

Los resultados principales corresponden a un modelo dinámico completo del extractor de energía y consejos de diseño importantes que permiten al diseñador lidiar con el sacrificio de potencia de salida al aumentar el rango de frecuencias sintonizable.

Keywords: Generación de Energía por Vibración, Modelación de sistemas dinámicos, Diseño Paramétrico

ABSTRACT

In this article we present the modeling and design guidelines for the development of a rotational electromagnetic vibration harvester. An important feature is that the special configuration of these harvesters allows them to be easily customized and tunable in a wide range of excitation frequencies. These harvesters are mainly intended for energizing wireless remote sensors mounted in critical but hard to reach points in heavy vehicles or in structures subject to strong vibrations.

Linear vibrations at a point of a vibrating structure are transformed into a rotational oscillation, so the natural frequency of the harvesting device depends on the moment of inertia rather than the mass of the moving parts. The moment of inertia can then be easily varied by relative displacement of the moving parts respect to the rotational oscillation pivot, and hence the natural frequency of the harvester can be tuned.

The main results correspond to a complete dynamical model of the harvester and critical design considerations that allows the designer to deal with the trade-off between range of frequencies and power output

Keywords: Vibration Energy Harvesting, Dynamic System Modelling, Parametric Design

NOMENCLATURE

WSN	Wireless Sensor Network
VEH	Vibration Energy Harvester
FEM	Finite Elements Method
RMS	Root Mean Squared
Nz	Number of turns along z axis of the coil
Nr	Number of layers along r axis of the coil
K_ϕ	Electromagnetic coupling coefficient
z_{mag}	Position of magnet relative to coil
R_{mag}	Magnet radius
h_{mag}	Magnet height
$airgap$	Radial distance between magnet and coil
B_r	Magnet remanence
d	Copper wire diameter
h_{coil}	Coil height
r_k	Radial position of each wire turn.
z_j	Vertical position of each wire turn.
P_{coil}	Electrical power dissipated in coil resistance
R_{coil}	Coil electric resistance
ε_{in}	Induced voltage in coil
I	Electric current
F_M	Magnetic force developed for coil-magnet interaction
v_{mag}	Magnet speed relative to coil
c_p	Parasitic damping
F_e	Excitation force
θ	Pivoting arm angle relative to the device structure
y_1	Position of the device relative to ground
M	Moving mass used to tune frequency

L_M	Tuning mass position
L_1	Pendulum length
L_5	Pivoting arm height
L_7	Device height
k	Stiffness of springs
M_{mag}	Magnet mass
y_{mag}^{base}	Position of magnet relative to the base of the device
θ_0	Equilibrium angle of the pivoting arm
ϑ	Pivoting arm angle relative to equilibrium angle
R_L^*	Optimal electric load
$P_L(R_L^*)$	Optimal average power at optimum electric load
C	Friction of the system
ζ	Critical damping factor
f_0	Natural frequency of the device
l_m	Position of tuning mass normalized by L_1
l_{cg2x}	Position of the center of mass of pivoting arm
l_k	Position of springs normalized by L_1
S	$=kl_k^2$, Equivalent stiffness normalized by L_1^2
ρ	M/M_{mag} ratio
δ	M_2/M_{mag} ratio
i_m	Inertia of mass M normalized by ML_1^2
i_m	Inertia of pivoting arm normalized by $M_2L_1^2$
ϑ_{max}	Maximum amplitude of $\vartheta(t)$ relative to θ_0
σ	L_5/L_7 ratio
τ	Minimum value of y_{mag}^{base}/L_7

1. ARTICLE BACKGROUND

1.1. Introduction

This thesis is one the outcomes of the FONDEF project D10I1069 “Multiphysics real time simulation models applied to the condition based maintenance and predictive maintenance of big sized mobile machinery”.

The objective of that project is to use the real time operational data of large vehicles to determine the condition of its components and to schedule optimal maintenance actions, saving time and money.

Electric energy is required for using specialized sensors and wireless communication hardware on condition monitoring. This energy source has to be independent from the vehicle electronics, easy to install, autonomous and robust.

Large vehicles, like mining trucks or defense tanks, are generally subject to strong vibrations produced by the roughness of the ground where they work. Thus one option, to energize the wireless sensor system, is to use a vibration energy harvester (Zuo & Zhang, 2013).

Energy harvesting from ambient sources has been a growing research field in the latest 15 years (Borca-Tasciuc et al., 2010), in particular for the development of wireless sensor networks (WSN). WSN covers a wide range of applications including structures monitoring, environment measurements, biometrics, security, animal population control and defense (Zahid Kausar et al., 2014).

Typical solutions for vibration energy harvesters include devices which resonate with the input vibration and convert the resultant mechanical energy into electrical energy. Mechanical can be converted to electrical energy in several ways such as through piezoelectric materials (Xiao & Wang, 2014), or electromagnetic generators based in

Faraday's law (Cepnik et al., 2013), or variable capacitance devices (Boisseau et al., 2012) or magnetostrictive materials (Wang & Yuan, 2008).

Maximum power output occurs at resonance (Williams & Yates, 1995). Different techniques, such as natural frequency tuning or widening of the bandwidth of the response, have been developed to reach maximum power (Zhu et al., 2010).

This thesis presents the design of an electromagnetic energy harvester with a tunable natural frequency. The device works like a horizontal pendulum, a pivoting arm held by springs coupled with a coil-magnet linear generator and a moving mass. The natural frequency is tuned by changing the position of that mass along the arm, which changes the effective mass of the system. A novel feature of the proposed design is that it keeps the equilibrium position of the oscillation of the magnet in certain point with respect to the coil, maximizing the power output.

The next sections of this chapter are structured as follows: Section 1.2 defines the main objectives of this work; Section 1.3 states the hypothesis of this thesis; Section 1.4 presents a literature review of the different alternatives of vibration energy harvesters to feed wireless sensor networks. Section 1.5 exposes the main conclusions of the present research, and Section 1.6 briefly presents the further research.

Chapter 2 exposes the main body of this thesis structured as a journal article. Within it, Section 2.1 introduces the theoretical background, Section 2.2 presents the proposed device, Section 2.3 develops the modeling of the coil-magnet interaction and equations of motion of the device, Section 2.3 presents the validation of the expressions used for the coil-magnet interaction, Section 2.4 presents critical design considerations, Section 2.5 shows experimental results to validate the design proposed, Section 2.6 discusses the main results, and finally Section 2.7 summarize the main findings and present the conclusions that can be drawn.

1.2. Main Objectives

The main objective of this work is to obtain a mathematical model of a rotary electromagnetic tunable vibration energy harvester based on a simple coil-magnet linear generator. The model will be useful to predict the response of the device and to design it for a specific application.

To achieve this goal, the following specific objectives were defined:

- To obtain a simple mathematical model for the electromechanical interaction between a cylindrical magnet and a coil with relative movement between them.
- To obtain a general dynamic model of the proposed device based on the coil-magnet interaction, useful to predict the power output and range of natural frequencies of the device.

1.3. Hypothesis

Obtaining the non-linear mathematical model of a new type of vibration energy harvesters allows to find a set of design variables that maximizes the power output and extends the range of operational excitation frequencies. This new harvester has design features that improve its performance. Although simple in terms of fabrication, the behavior of the system is governed by a set of non-linear differential equations, which can be derived from dynamics and electromagnetic principles. These equations can be solved numerically using time integration schemes in order to accurately predict performance and efficiency. The model can be validated experimentally using suitable data acquisition techniques and hardware and the degree of accuracy can be ascertained.

1.4. Literature Review

1.4.1. Wireless Sensors Networks

A group of sensor nodes communicating through wireless channels, deployed in a region for sensing different variables of interest constitute a Wireless Sensor Network (WSN) (Akhtar & Husain, 2015; Mathúna et al., 2008; Zahid Kausar et al., 2014).

The concept behind WSN is to obtain non-centralized information about a region, process or structure, so the sensing nodes have to be deployed and work independently, sending data to a central unit. The "independent" characteristic is related to the power source. The power source has to be sufficiently efficient to manage the power stored in a battery to last weeks or even months. To overcome that problem, power could be obtained from the environment in which the sensor is deployed.

Different ways to energize a WSN are shown in Figure 1-1. The selected source will depend on the application and the availability of the power source.

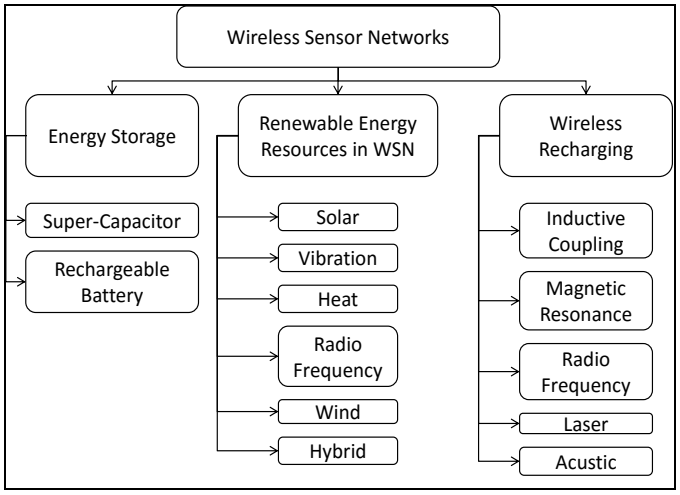

Figure 1-1: Classification of energy storage, renewable energy resources and wireless recharging from renewable and traditional energy resources in WSNs (Akhtar & Husain, 2015).

At this point, available commercial sensor networks nodes have reached very low energy consumption that makes feasible the application of WSN. For example, the Crossbow MICA has an average of 2.8mW of consumption with a data rate of 250kbps at typical range of 100m in outdoor environments or 30m indoor (Zahid Kausar et al., 2014).

1.4.2. Vibration Energy Harvesting

Vibration energy can be found in different applications such as industrial machinery, vehicles (automobiles, trucks, helicopters and airplanes), civil structures, human or animal motion as in ocean waves. The main differences between the different sources of vibration are the magnitude and type of excitation, which could be periodic or stochastic (Tang et al., 2010). If the excitation is periodic, there is a fundamental frequency of excitation which could be fixed or variable in time.

The general structure of a Vibration Energy Harvester (VEH) is showed in Figure 1-2.

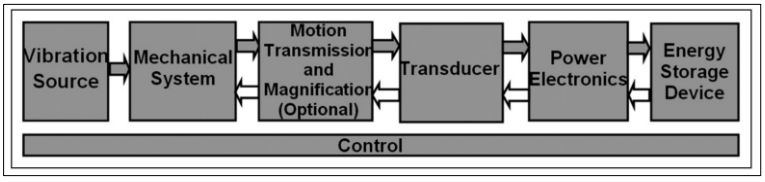

Figure 1-2: Typical components of a vibration energy harvesting system (Zuo & Tang, 2013).

The vibration is transferred to a transducer through a mechanical system which may have a magnification mechanism. The transducer is the component that transforms kinetic energy in electric energy.

The type of mechanical system used in the VEH will depend on the transduction mechanism. There are devices based on mechanical strain that uses smart materials like piezoelectric or magnetostrictive materials, while those which rely on relative velocity

between two bodies are associated with electromagnetic generators. Relative position is associated with electrostatic transduction (Beeby et al., 2006).

Piezoelectric effect occurs in special materials, like Zirconate Titanate (PZT) or Piezo-polymer Polyvinylidene Fluoride (PVDF), that produce an electric charge when stressed (Akhtar & Husain, 2015; Khaligh et al., 2010). Figure 1-3 shows different configurations used at this time.

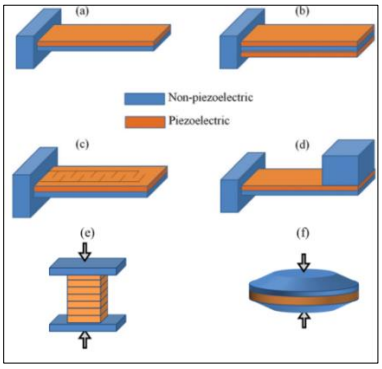

Figure 1-3: Various configurations of piezoelectric harvesters: (a) unimorph; (b) bimorph; (c) a piezoelectric cantilever with interdigitated electrodes; (d) a piezoelectric cantilever with proof mass at its free end; (e) multilayer stack; (f) cymbal type with a piezoelectric disc. Adapted from (Li et al., 2014)

Magnetostrictive materials, like the Metglas 2605SC, produce a magnetic field when stressed. That magnetic field can be scavenged with a coil, but it needs magnets and an iron core to close the magnetic circuit (Wang & Yuan, 2008) as seen in Figure 1-4

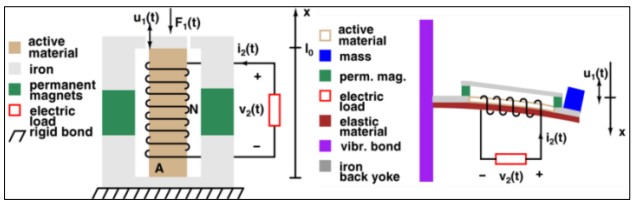

Figure 1-4: Direct force-driven magnetostrictive concept (left) and an Inertial velocity-driven concept (right). Adapted from (Davino et al., 2012)

Electrostatic harvesters generate voltage based on the displacement of the plates of a charged capacitor. The relative movement opposes the force of electrostatic attraction producing the conversion of vibrational energy in energy stored in the capacitor's electric field (Mathúna et al., 2008). Different ways of obtain that relative displacement are showed in Figure 1-5.

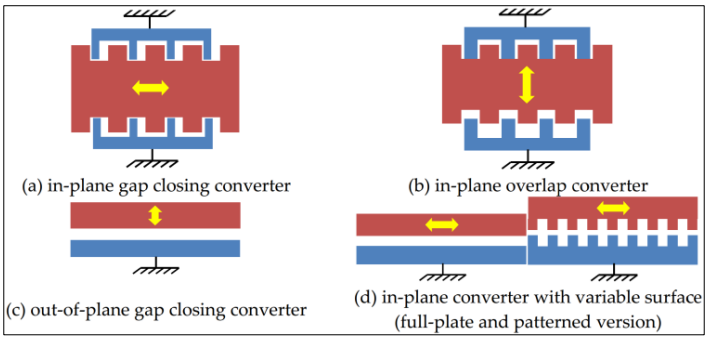

Figure 1-5: Basic capacitor shapes for electrostatic converters (Boisseau et al., 2012)

Finally, electromagnetic energy harvesters are based on Faraday's law of induction. Permanent magnets in relative motion to a coil or a coil array induce a voltage proportional to the speed of the magnetic flux change inside the coil. Different configurations of permanent magnet generators have been developed as shown in Figure 1-6.

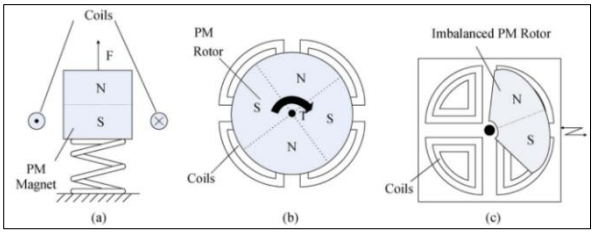

Figure 1-6: Three different categories of PM power-generator topologies. (a) Resonant generator operating in oscillating mode under vibration force. (b) Rotational generator operating under steady torque. (c) Hybrid generator to convert linear motion into rotational motion. Adapted from (Khaligh et al., 2010)

The main advantages and drawbacks of each transduction mechanism are compared in Table 1-1.

Table 1-1: Comparison of the different vibration energy harvester mechanisms. Adapted from (Boisseau et al., 2012; Wang & Yuan, 2008).

Type	Advantages	Drawbacks
Piezoelectric	-high output voltages -high capacitances -compact configuration -compatible with micro-scale devices -high coupling -no external voltage source	-depolarization -brittleness in bulk piezo-layer -poor coupling in piezo-film (PVDF) -charge leakage -high output impedance -expensive material
Magnetostrictive	-ultra high coupling coefficient -high voltages -no polarization problem -high flexibility -suited to high frequency vibration	-nonlinear effect -pick-up coil -may need bias magnets -difficult to build at micro-scale
Electrostatic	-high output voltages -no need for smart material -easy to implement at micro-scale -high output voltages -low cost -coupling coefficient easy to adjust -high coupling coefficient reachable -size reduction increases capacitances	-low capacitances -high impact of parasitic capacitances -external voltage source -mechanical constraints needed
Electromagnetic	-high output current -robustness -proven long lifetime -no need of smart material -no external voltage source -better power density at macro-scale	-low output voltages -hard to develop micro-scale devices -low efficiency in low frequencies and small sizes

1.4.3. Tubular type electromagnetic vibration energy harvester

In this section we discuss basic VEH theory applied to an elemental configuration as shown in Figure 1-7. Here, a cylindrical magnet slides inside a copper coil. The magnet is supported by a helical (linear) spring having constant k. Air friction and sliding friction are modeled by the parasitic damping coefficient c_P. The electromagnetic interaction between magnet and coil produces a force F_M opposing the motion of the moving magnet.

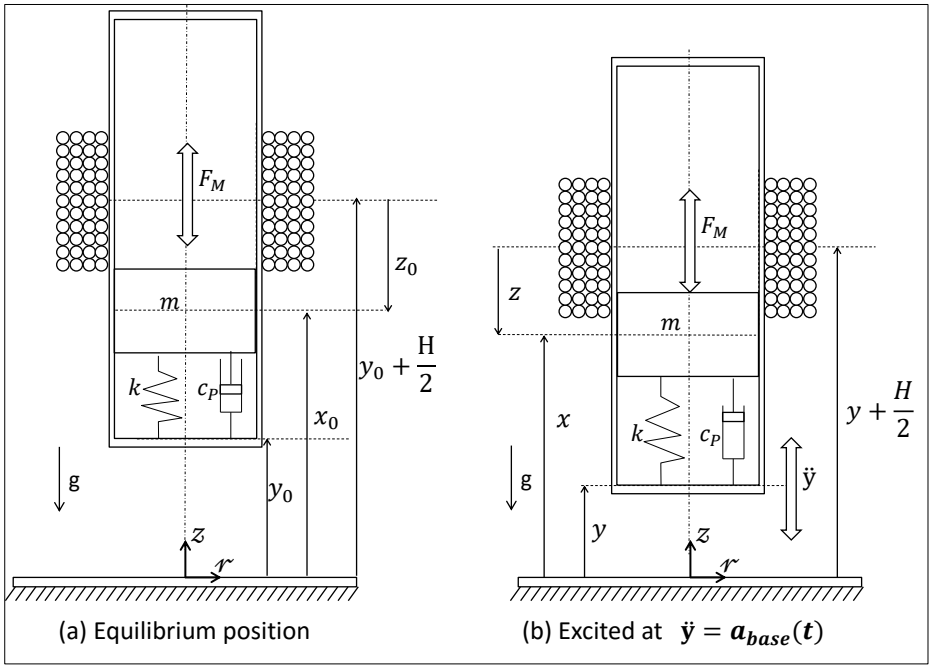

Figure 1-7: Tubular type electromagnetic vibration energy harvester in equilibrium position (a) and when excited by an acceleration at its base (b)

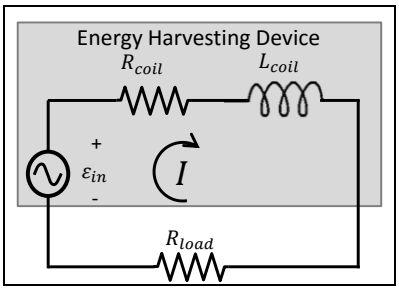

Figure 1-8: Electric model of the electromagnetic energy harvester.

Figure 1-8 shows the equivalent circuit. Extracted energy is that dissipated by resistance R_{load}. Coil internal resistance and inductance are modeled by R_{coil} and L_{coil} respectively.

Applying dynamic equilibrium equations and using a change of variable $z - z_0 = (y - y_0) - (x - x_0)$ gives

$$m\ddot{z} + c_p\dot{z} + k(z - z_0) = m\ddot{y} + F_M(t) = F_e(t) + F_M(t) \tag{1.1}$$

If z_{mag} is the position of the magnet relative to the coil then the following state space dynamic model is obtained:

$$\dot{z}_{mag} = v_{mag}$$

$$\dot{v}_{mag} = \ddot{y}(t) + \left(-c_p v_{mag} + -k(z - z_0) + F_M\right)/m \tag{1.2}$$

$$\dot{I} = \left(\varepsilon_{in} - I(R_{load} + R_{coil})\right)/L_{coil}$$

Variable v_{mag} is the instantaneous velocity of the magnet and $\ddot{y}(t)$ is the acceleration of the structure being harvested.

Magnetic force F_M and induced voltage ε_{in} are computed using an electromagnetic coupling coefficient K_ϕ that is derived from Faraday's law of induction.

$$\varepsilon_{in} = v_{mag}K_\phi \tag{1.3}$$

$$F_M = IK_\phi \tag{1.4}$$

1.4.4. Conditions for maximum energy extraction

Conditions for maximum power extraction have been analyzed by several authors (Mitcheson et al., 2004; Saha et al., 2006; Stephen, 2006; Williams et al., 2001). Our analysis follows Stephen's approach (Stephen, 2006) which is to consider the average power output as the energy dissipated by the external resistance R_{load}.

Damping produced by the electromagnetic coupling is taken into account by factor c_M . It considers the energy dissipation by the external resistance R_{load} and the internal coil resistance R_{coil}. Then, the magnetic force can be computed as the product of c_M and the relative velocity of the magnet,

$$F_M = c_M \dot{z}_{mag} \tag{1.5}$$

Assuming that the coil self inductance is negligible then,

$$c_M = c_{coil} + c_L = \frac{K_\phi \left(z_{mag}\right)^2}{R_{coil} + R_{load}} \tag{1.6}$$

Where,

$$c_L = R_{load} \frac{K_\phi \left(z_{mag}\right)^2}{(R_{coil} + R_{load})^2} \;\; ; \;\; c_{coil} = R_{coil} \frac{K_\phi \left(z_{mag}\right)^2}{(R_{coil} + R_{load})^2} \tag{1.7}$$

Assuming that the external excitation acceleration to the system described in (1.1) is $\ddot{y}(t) = A \sin(\omega t)$, the solution to equation (1.1) is:

$$z_{mag}(t) = \frac{\frac{mA}{k}}{\sqrt{\left(1 - \frac{\omega}{\omega_0}\right)^2 + \left(2\zeta \frac{\omega}{\omega_0}\right)^2}} sin(\omega t - \varphi) \tag{1.8}$$

Where φ is the output phase angle and ζ is the critical damping coefficient of the system, and:

$$atan(\varphi) = \frac{2\zeta\left(\frac{\omega}{\omega_0}\right)}{\left(1-\frac{\omega}{\omega_0}\right)}\ ;\ \zeta = \frac{c_{eq}}{2\sqrt{km}}\ ;\ \omega_0 = \sqrt{k/m}\ ;\ c_{eq} = c_P + c_M \tag{1.9}$$

Then the average power output at the load resistance is given by:

$$P_L(\omega) = \frac{1}{T}\int_0^T c_L \cdot \left(\dot{z}_{mag}\right)^2 dt = \frac{1}{2}\frac{c_L m^2 \omega^2 A^2/k^2}{\left(1-\left(\frac{\omega}{\omega_0}\right)^2\right)^2 + \left(2\zeta\frac{\omega}{\omega_0}\right)^2} \tag{1.10}$$

The average power output is maximum when $\omega_0 = \omega$, but also R_{load} must meet a given condition. Under resonance (1.10) becomes:

$$P_L(R_{load}) = \frac{1}{2}\frac{c_L(R_{load}) m^2 \omega_0^2\, A^2/k^2}{(2\zeta)^2} = \frac{c_L}{2}\frac{m^2 A^2}{c_{eq}^2} \tag{1.11}$$

The optimal value of R_{load} is given by

$$R_L^* = \frac{1}{c_p}K_\phi^2 + R_{coil} \tag{1.12}$$

And then the maximum power that can be extracted is:

$$P_L(R_L^*) = \frac{1}{8}\frac{m^2 A^2}{c_p}\frac{1}{\frac{R_{coil}c_p}{K_\phi^2}+1} \tag{1.13}$$

1.4.5. Tunable vibration energy harvesters

Most of the VEH are composed of spring-mass systems which reach maximum performance at resonance, i.e. when their natural frequency matches the input vibration frequency. Generally, the frequency response of such devices is narrow, which means that if they do not work in resonance, the output power is dramatically decreased. A solution to this problem is to design a device capable of periodically tune its own natural frequency to match the frequency of the ambient vibration. Another solution is to widen the bandwidth of the generator. Periodic tuning can be realized by mechanical or

electrical methods while bandwidth widening can be achieved using different strategies as generator arrays, mechanical stoppers, nonlinear springs or bi-stable structures (Zhu et al., 2010).

Natural frequency of a second order linear system has the form $\omega = \sqrt{k/m}$ where k represents the stiffness of the system and m its effective mass. Mechanical tuning methods are based in changes of one of these parameters. For example changing the length of a cantilever VEH would modify its natural frequency, making it higher if it is shortened and vice versa.

Electrical tuning is based in changing the electrical damping by adjusting the load impedance which produces a shift in the power spectrum.

Bandwidth widening techniques are suitable when vibrations are mostly random and there is not a fundamental frequency governing the input excitation. Different techniques has been developed for example the use of arrays of resonant generators with different natural frequencies (multimodal energy harvesting) or the use of non-linear effects, like bi-stability or non-linear stiffness, which produces a wider power spectrum.

A comparison of different strategies used to increase the operational frequency range of a VEH is shown in Table 1-2 .

Table 1-2: Comparison of the different strategies for increase the operating frequency of VEH. Adapted from (Zhu et al., 2010).

Strategies	Advantages	Disadvantages
Mechanical Tuning	-High efficiency	-Extra system and energy are required -Responds to only one frequency at a time -Slow response to a change in a vibration frequency
Change dimension	-Does not affect damping	-Difficult to implement -Not suitable for tuning *in situ*
Change center of gravity	-Does not affect damping	-Not suitable for tuning *in situ*
Change spring stiffness continuously	-Suitable for *in situ* tuning	-Consumes energy when generator works at resonance
Apply axial load (change spring stiffness intermittently)	-Easy to implement -Suitable for *in situ* tuning -No energy is required when generators work at resonance -Damping is not affected when the tensile load is applied	-Increased damping when the compressive load is applied
Electrical Tuning	-Easy to implement -No energy is required when generator work at resonance -Suitable for *in situ* tuning	-Low tuning efficiency
Widen Bandwidth	-No tuning mechanism required -Respond to different frequencies at the same time -Immediate response to a change in vibration frequency	-Complexity in design
Generator array	-Damping is not affected	-Complexity in design -Low volume efficiency
Use mechanical stopper	-Easy to implement	-Fatigue problem -Decrease in maximum output power
Coupled oscillators	-Easy to implement	-Decrease in maximum output power
Nonlinear generators	-Better performance at excitation frequencies higher than resonant frequency	-Complexity in design -Hysteresis
Bi-stable structure	-Better performance at excitation frequencies much lower than resonant frequency	-Complexity in design

1.5. Related work and patentability

In this work, a horizontal pendulum vibration energy harvester is proposed. Similar devices with a hinged horizontal arm has been studied before, Appendix D shows some of them.

Moreover, a patent search (Appendix E) revealed that similar configurations had been patented but some aspects of the proposed work have enough novelty to be patented. Thanks to that fact the proposed design won the "IX CONCURSO DE PATENTAMIENTO" carried by the UC Research Vice-Rectory, and funding has been received for patentability studies. The forms presented are exposed in Appendix F.

The patentability of the proposed design is possible since the especial configuration to keep the magnet in an optimal resting position respect to the coil is an innovation respect to the state of the art that increases its power output, which was confirmed by a patent search carried out by specialists in intellectual property (Appendix G).

1.6. Main contributions

In this work the modeling, validation and design considerations of an electromagnetic horizontal pendulum vibration energy harvester were presented.

- An experimentally validated model of a tunable rotary vibration energy harvester with a coil-magnet linear transducer.
- A study of the trade-off between natural frequency and maximum mean power.
- Critical design guidelines for the proposed configuration, including explicit expressions for the natural frequency, power output, optimal load resistance and geometric constraints.

2. HORIZONTAL PENDULUM ELECTROMAGNETIC VIBRATION ENERGY HARVESTER WITH TUNABLE NATURAL FREQUENCY: MODELING AND DESIGN

2.1. Introduction

Obtaining information from remote or hard to reach systems in real time using Wireless Sensor Networks (WSN) has gained great importance in past few years in a variety of applications such as in monitoring structures and vehicles, the environment, biometrics, security and military applications (Mathúna et al., 2008; Zahid Kausar et al., 2014).

Tied to this interest of obtaining field information is the need to power these data acquisition systems, where it is increasingly necessary to extend autonomy and independence from the mains.

The concept of vibration energy harvesting finds here an application since many of these remote data acquisition systems are near some kind of mechanical system in motion from where energy can be harvested (Beeby et al., 2006; Weddell et al., 2012).

Numerous devices based on either piezoelectric, electrostatic, or electromagnetic principles have been developed having design objectives such as small size, high power and extended frequency range of operation (Galchev et al., 2011), for which different techniques have been proposed depending if the excitation source has a fixed, variable or stochastic frequency (Tang et al., 2010).

One of the conditions for maximum power extraction is that the natural frequency of the energy extracting device matches the excitation source frequency. Depending if the excitation frequency is fixed or variable, it will be necessary to adjust the natural frequency of the energy harvesting device manually or automatically (Zahid Kausar et al., 2014). It is necessary to consider that the energy necessary to adjust the frequency of

the harvesting device could well exceed the energy output obtained, for which then a suitable strategy for adjustment must be designed (Eichhorn et al., 2011) .

An energy harvester with tunable natural frequency is probably the best solution for powering sensors in heavy off road vehicles such as mining trucks, battle tanks, and general earthmoving vehicles, for implementing a condition based maintenance scheme. The vertical axis vibration produced by the motion of the vehicle while traveling along the road, both in frequency and amplitude depends on the road roughness and the instantaneous speed. A model of this is analyzed in (Zuo & Zhang, 2013) and several simulation results are given in (Agostinacchio et al., 2013; Reza-Kashyzadeh et al., 2013; Zhou et al., 2009). Low frequency vibrations are generally the most important in the spectrum (between 1-30 Hz), depending also in the moving mass and the damping system (Gagliardi & Utt, 1993).

In this article we present a novel configuration for vibration energy harvesting consisting in a flat platform base that supports a pivoted horizontal beam with a magnet coil assembly at one end, a moving mass along the beam, and springs connected to variable positions between the platform base and beam. The moving mass allows to modify the natural frequency of the device. The vibration of the platform base induces a relative motion between coil and magnet producing an output voltage. An important novelty is that the natural frequency of the device can be tuned to the external excitation frequency device and also to maintain a fixed equilibrium position in the coil-magnet assembly. This is very important since the magnet needs to oscillate respect to the rim of the coil in order to maximize voltage output.

The objective of this work is to obtain a mathematical model of the proposed configuration that includes the dynamic equations that govern the motion of the moving parts and also the nonlinear behavior of the coil-magnet assembly, in order to predict its range of frequencies and power output.

Section 2.2 exposes the principles of operation of the proposed device. Section 2.3 includes mathematical expressions for voltage generation, magnetic force, maximum power extraction conditions and the equations of motion of the device.

Section 2.4 discusses important design issues such as the selection of a design frequency range, trade-off between range of frequencies and output power, and geometric constraints.

Section 2.5 shows experimental validation of the coil-magnet interaction, and experimental verification of the expressions given for the natural frequency, equivalent stiffness and equilibrium position. The critical damping factor calculation method used is presented also in this section.

Section 2.6 presents a discussion of the main results and finally section 2.7 summarize the main conclusions and future work.

Finally Section 3.1 gives comments about the patentability of the proposed design and Section 3.2 summarizes the main findings.

2.2. Harvester Design

The end goal of this research is to harvest energy from vibrations of variable amplitude and frequency such as those coming from a moving vehicle. For maximum energy extraction two important conditions that any suitable device must meet are a) the device must self-adjust its natural frequency to match the instantaneous excitation frequency, and b) it must maintain the equilibrium position of the coil-magnet assembly with the magnet oscillation centered about the rim of the coil if the coil is larger than the magnet, or centered about the center of the coil if the magnet is larger than the coil, because these give the maximum magnetic flux magnitude (Berdy et al., 2014; Spreemann & Manoli, 2012).

Figure 2-1 shows a harvester configuration devised by the authors. The moving mass allows to adjust the natural frequency of the device, but when the mass moves the coil, magnet resting position must be reset by moving the coil, so that the oscillation of the magnet remains centered about the rim of the coil.

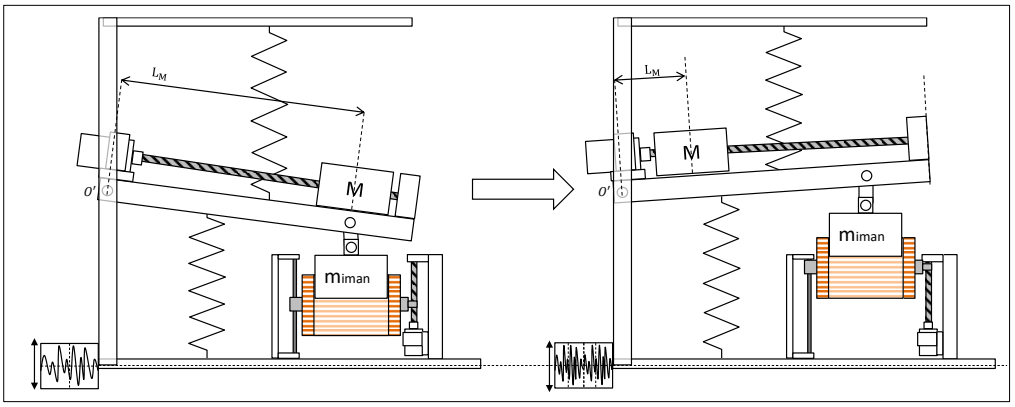

Figure 2-1: Proposed device

The device includes an oscillating arm pivoted at point O'. Two extension springs give additional support to the arm to help maintain a near horizontal rest position. A moving mass M has an instantaneous position L_M that allows to adjust the natural frequency. A magnet is held at the extreme end of the arm and hence can oscillate relative to the coil.

2.3. Modeling

In this section we model the interaction between coil and magnet. In spite of its geometric simplicity it is the most complex aspect of the entire mathematical model of the system. Non-trivial expressions are derived to compute induced voltage and magnetic force.

Next the conditions for maximum power output are presented according to the nomenclature used in this article

2.3.1. Coil-Magnet Interaction

A critical part in the energy generation system is the coil-magnet interaction. A design methodology should have the simplest equations possible in order to allow for fast design iteration and optimal design variables search. Suitable analytic expressions are needed to compute the induced voltage and also the electromagnetic force acting.

Authors have used expressions with different levels of complexity, from linearized (Cepnik et al., 2011; Mitcheson et al., 2004), to nonlinear as given by the Maxwell equations (Avila Bernal & Linares García, 2012; Berdy et al., 2014; H. Liu et al., 2013; Peralta et al., 2014). Magnetic circuits approach has also been used for modelling devices with linear generators that take advantage of materials with high magnetic permeability and arrays of multiple magnets (Jiang et al., 2013; Patel & Khamesee, 2013; Zeng & Khaligh, 2013).

The use of FEM software makes it possible to analyze complex geometries with accuracy (Howard et al., 2013; Mccarthy et al., 2008; Munaz et al., 2013; Zeng & Khaligh, 2013), however this approach is time consuming, hence not so amenable for design optimization purposes.

In this work we decided to use an analytical model with intermediate level of complexity in order to consider nonlinear effects but with low implementation and evaluation time. The approach is to model the magnetic field produced by a cylindrical magnet and then calculate the magnetic coupling by means of the Faraday's law of induction. This approach is suitable since the relative magnetic permeability of air, copper and neodymium are near from 1. Air gap influence is implicit in the model.

In (Hawley, 2012) expressions can be found for computing the magnetic field density produced by a cylindrical permanent magnet by two methods: method of current surface density and the method of magnetic monopoles, and there equivalence is proven. In (Ravaud et al., 2010) expressions are given for the magnetic flux, magnetic force, inductance obtained by elliptical integrals, which reduces notably the computation time

relative to the use of iterative methods. These are further simplified in (Robertson et al., 2011).

In implementing the approach suggested in (Ravaud et al., 2010; Robertson et al., 2011) singularities were found, which even though provided with a solution by the authors, still produced instabilities in the neighborhood so were found not so efficient for design purposes. For this reason the method proposed in (Hawley, 2012) was preferred, which requires some numerical integration but nonetheless resulted in a more robust solution.

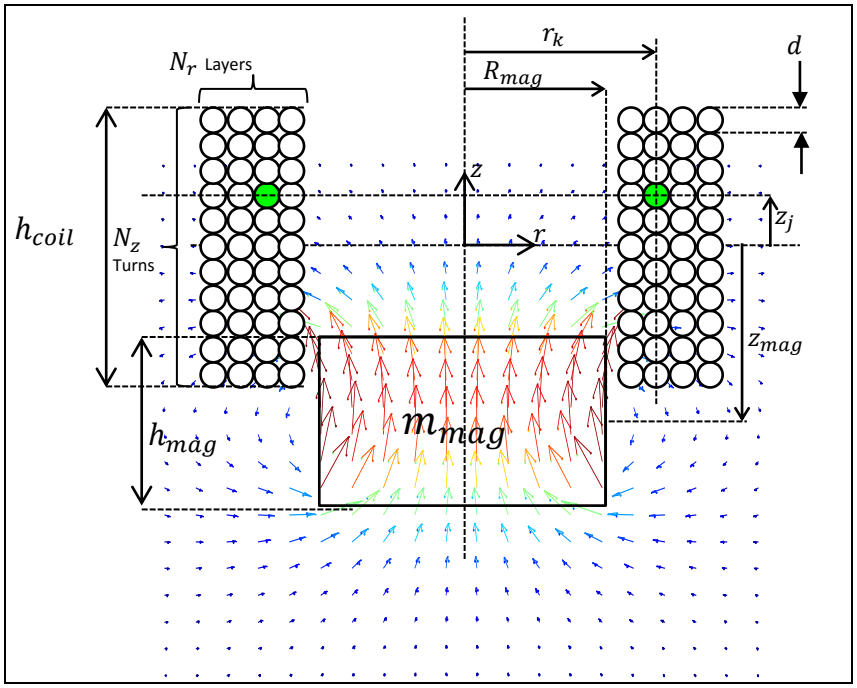

Figure 2-2: Geometric parameters used to model the induced voltage in the magnet-coil system. Colored arrows indicate the magnetic flux density, which was plotted using expressions found in (Hawley, 2012).

The induced voltage ε_{in} for the system described in Figure 2-2 can be calculated applying Faraday's law at each wire loop and adding the contribution of each one. The magnetic flux ϕ in every turn can be computed by a double integral inside the wire loop area, where only the $\hat{\mathbf{z}}$ direction of the magnetic density flux of the magnet will contribute effectively and the resultant flux depends on the relative position between the

magnet and coil. The final expression for ε_{in}will depend on the speed of the magnet relative to the coil and a magnetic coupling term K_ϕ.

$$\varepsilon_{in} = -\sum^{Nz}\sum^{Nr}\frac{d\phi}{dt} = -\sum^{Nz}\sum^{Nr}\iint\frac{dB^z_{mag}(z_{mag})}{dt}dA = -\dot{z}_{mag}K_\phi\left(z_{mag}\right) \quad (2.1)$$

The term K_ϕ is called the magnetic coupling constant and depends only on the relative position z_{mag} between magnet and coil.

The above expression can be expanded using expressions for B^z_{mag} given by (Hawley, 2012), then:

$$K_\phi(z_0) = -2\pi\frac{B_r R_{mag}}{4\pi}\sum_{i=1}^{N_r}\sum_{j=1}^{N_z}\int_0^{r_k}\int_0^{2\pi}\left(\frac{\left(R_{mag}-r\cos(\psi)\right)}{\left(r^2+{R_{mag}}^2+\left(z_{mag}+\frac{h_{mag}}{2}-z_j\right)^2-2R_{mag}r\cos(\psi)\right)^{\frac{3}{2}}}\right.$$
$$\left.-\frac{\left(R_{mag}-r\cos(\psi)\right)}{\left(r^2+{R_{mag}}^2+\left(z_{mag}-\frac{h_{mag}}{2}-z_j\right)^2-2R_{mag}r\cos(\psi)\right)^{\frac{3}{2}}}\right)r\,d\psi\,dr \quad (2.2)$$

Where (r_k, z_j) is the position of a given turn in cylindrical coordinates, and B_r is the magnet remanence.

The above expression allows to compute the magnetic coupling value considering the coil-magnet assembly geometry.

The amount of time required to evaluate the above expression in its original form makes it inconvenient for design purposes, so it is solved in an approximate but more practical approach.

We will use (2.2) by pre computing values for a number of different magnet and in dynamic simulation we will interpolate using a mathematical adjusted curve of the following form:

$$\mathrm{K}_{\phi}^{*}(\mathrm{A},\mathrm{B},\mathrm{C},\mathrm{z}) = \frac{\mathrm{A}}{((\mathrm{z}-\mathrm{B})^2+\mathrm{C})^{\frac{3}{2}}} - \frac{\mathrm{A}}{((\mathrm{z}+\mathrm{B})^2+\mathrm{C})^{\frac{3}{2}}} \tag{2.3}$$

An expression for the magnetic force is obtained by considering that the work done in a displacement dz during a time interval dt is equivalent to the instantaneous power developed, hence:

$$P_{coil} = \varepsilon_{in} I = F_M(z_{mag}) v_{mag} \tag{2.4}$$

$$F_M(z_{mag}) = \frac{\varepsilon_{in}}{v_{mag}} I = -K_{\phi}(z_{mag}) I \tag{2.5}$$

Computing the force in this manner greatly simplifies the optimal design search when compared to using expressions such as given in (Ravaud et al., 2010; Robertson et al., 2011), given their complexity and existence of mathematical singularities.

In section 2.5.2 we will validate this simplification approach by comparing results obtained by the original equations as well as by FEM.

2.3.2. Conditions for maximum energy extraction

The conditions for maximum energy extraction have been analyzed by several authors, among them (Mitcheson et al., 2004; Saha et al., 2006; Stephen, 2006; Williams et al., 2001). We follow the approach by (Stephen, 2006) because it considers the usable extracted energy provided by R_{load} instead of the total energy dissipated by the system.

According to (Stephen, 2006) the optimal value of R_{load} (Figure 1-8) is

$$R_L^* = \frac{1}{c_p} K_{\phi}^2 + R_{coil} \tag{2.6}$$

With the above value the expression for optimal average power is

$$P_L(R_L^*) = \frac{1}{8} \frac{\max(F_e)^2}{c_p} \frac{1}{\frac{R_{coil} c_p}{K_{\phi}^2} + 1} \tag{2.7}$$

The above expression suggests that factor $R_{coil}c_p/{K_\phi}^2$ must be as small as possible. Hence it is desirable that the coil-magnet assembly must be designed trying to obtain the highest value of K_ϕ and lowest value of R_{coil} as proposed by (Saha et al., 2006).

However, since $K_\phi(z_{mag})$ is not constant a representative value must be used, for example its maximum value.

2.3.3. Derivation of the Equations of Motion

In this section the equations governing the motion are formulated using Lagrange´s Method.

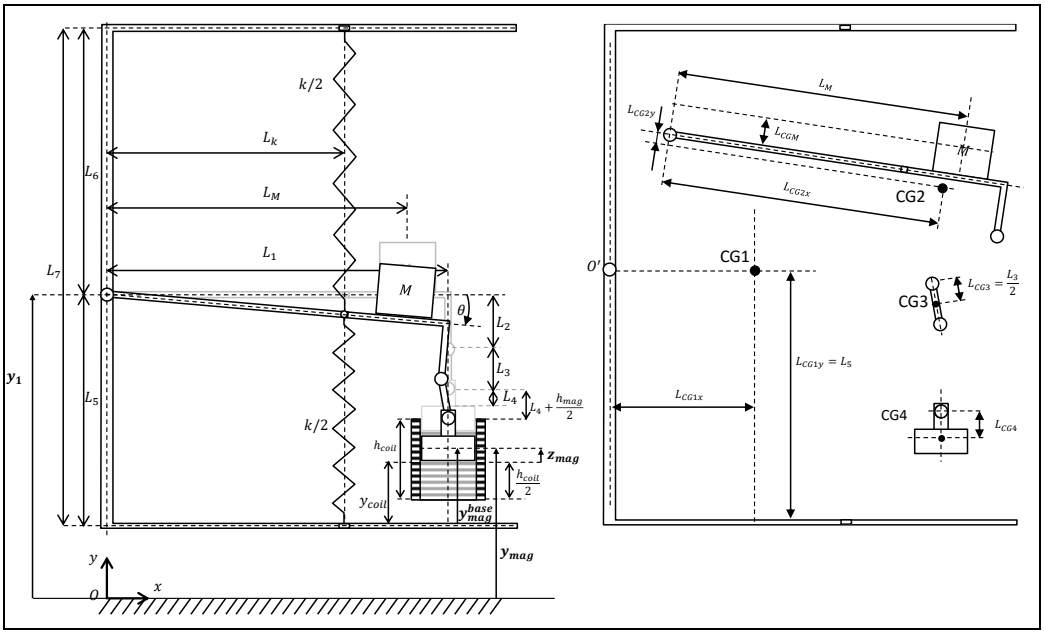

Figure 2-3: Parameters used to obtain a model the proposed device.

As shown in Figure 2-3, we choose $\{\theta, y_1\}$ as the set of generalized coordinates. The following assumptions are made:

a. Acceleration $\ddot{y_1}$ is known along the vertical axis.
b. The resulting spring constant for both springs is k.

c. Aerodynamic friction is considered mainly due to airflow between magnet and coil.
d. Oscillations are in the low frequency range and the self inductance of the coil is negligible.
e. For computational convenience, a constant value of K_ϕ will considered which will be computed as described earlier.

To obtain usable design equations masses of small linkages are considered negligible. Using Maple software for symbolic algebra processing gives as a result the following dynamic equation:

$$\begin{aligned}&\left(L_1^2 M_{mag} + L_M^2 M + M L_{CGM}^2 + L_{CG2x}^2 M_2 + L_{CG2y}^2 M_2 + I_2 + I_M\right)\boldsymbol{\alpha} \\ &\quad + \left(\left(L_{CG2y} M_2 - M L_{CGM} + L_2 M_{mag}\right)(\ddot{\mathbf{y}}_\mathbf{1} + g) + L_k^2 k - F_M L_2\right)\boldsymbol{\theta} \\ &\quad + \left((L_2^2 - L_1^2)\boldsymbol{\theta} - L_1 L_2\right) M_{mag}\boldsymbol{\omega}^2 + L_1^2 C\boldsymbol{\omega} + -g L_1 M_{mag} \\ &\quad + -L_M M g - g L_{CG2x} M_2 + L_k \frac{k}{2}\,(L_6 - L_0) - L_k \frac{k}{2}(L_5 - L_0) \\ &\quad = (L_M M + L_{CG2x} M_2)\ddot{\mathbf{y}}_\mathbf{1} + L_1 \ddot{\mathbf{y}}_\mathbf{1} M_{mag} - F_M L_1\end{aligned} \tag{2.8}$$

In static equilibrium the arm rests at an angle θ_0 given by:

$$\theta_0 = \frac{\left(L_M M + M_{mag} L_1 + L_{CG2x} M_2\right) g + (L_5 - L_6) L_k k/2}{L_k^2 k - M g L_{CGM} + M_{mag} g L_2 + M_2 g L_{CG2y}} \tag{2.9}$$

Considering a variable change of the type $\vartheta = \theta - \theta_0$, we can write

$$m_{eq}\frac{d^2\boldsymbol{\vartheta}}{dt} + c_{eq}\frac{d\boldsymbol{\vartheta}}{dt} + k_{eq}\boldsymbol{\vartheta} = F_e(\boldsymbol{t}) \tag{2.10}$$

Where,

$$\begin{aligned}&m_{eq} = \left(L_1^2 M_{mag} + L_M^2 M + L_{CG2x}^2 M_2 + I_2 + I_M\right)\ ; c_{eq} = c_p + c_M = C L_1^2 + \\ &\frac{K_\phi^2}{R_{coil}+R_{load}} L_1^2\ ; k_{eq} = L_k^2 k\ ;\ F_e(t) = \left(L_M M + L_{CG2x} M_2 + L_1 M_{mag}\right)\ddot{\mathbf{y}}_\mathbf{1}\end{aligned} \tag{2.11}$$

Replacing expressions above in equations (2.6) and (2.7), the following optimum values are obtained:

$$R_L^* = \frac{1}{C}K_\phi^2 + R_{coil} \tag{2.12}$$

$$P_L(R_L^*) = \frac{1}{8}\frac{(L_M M + L_{CG2x}M_2 + L_1 M_{mag})^2 \max(\ddot{y}_1)^2}{CL_1^2}\frac{1}{\frac{R_{coil}C}{K_\phi^2}+1} \tag{2.13}$$

Friction coefficient C can be estimated using equation (2.14). In this expression, values of ζ in the range 1% to 10% can be used, and later corroborated experimentally.

$$C = \frac{2\zeta\sqrt{k_{eq}m_{eq}}}{L_1^2} \tag{2.14}$$

The position z_{mag} of the magnet with respect to the coil is needed to calculate K_ϕ, hence,

$$z_{mag}(\theta) = L_5 - y_{coil} - L_1\sin(\theta) - L_2\cos(\theta) - L_3 - L_4 - \frac{h_{mag}}{2} \tag{2.15}$$

The vertical position of the magnet center relative to the base is needed to formulate geometric restrictions, and is given by:

$$y_{mag}^{base}(\theta_0) = L_5 - L_1\sin(\theta_0) - L_2\cos(\theta_0) - L_3 - L_4 - \frac{h_{mag}}{2} \tag{2.16}$$

2.4. Important Design Considerations

In this section important design issues are discussed, arising from the proposed device configuration.

2.4.1. Selection of frequency range

In order to design a harvester for a particular application, measurements have to be done in the vibration source which would give information about the magnitude and the frequency.

As an example, z axis vibration field data of a mining truck is shown. The sampling frequency was 100 [Hz] and a lowpass filter of 25 [Hz] was applied to the incoming signals for cleaning purposes.

In Figure 2-4 is shown the spectrogram of more than one hour of data and a selected time window, which FFT shows a predominant frequency at 6.22 Hz, consistent with a peak zone visible in the spectrogram.

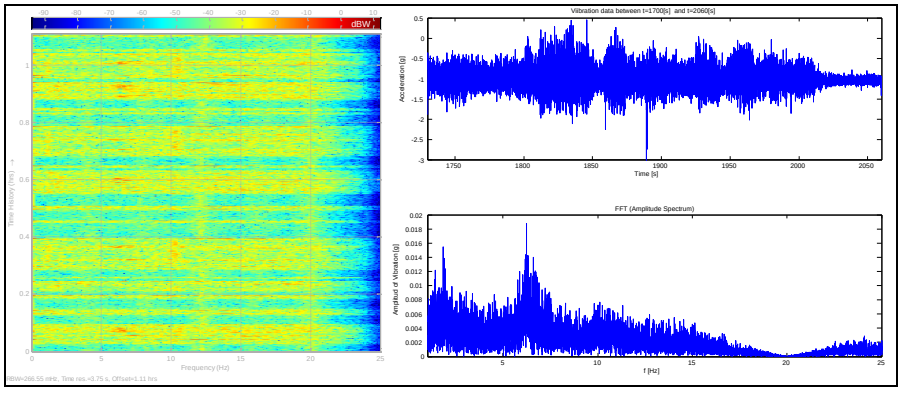

Figure 2-4: Measurements of vibration in the ‘z’ axis on a mining truck. At left the spectrogram of the measurements and at right a selected time window with its FFT.

2.4.2. Trade-Off between Maximum power extraction and working range of frequencies

It must be noted that a trade-off exists between power extraction and working range of frequencies. As the moving mass moves towards the pivot point, m_{eq} decreases, and as a consequence the power extraction diminishes according to equation (2.13). At the same time as the moving mass moves towards the pivot the natural frequency of the device increases. As a result, to extend the working frequency range requires a sacrifice in the maximum power that can be extracted.

To understand the nature of this trade-off, let us first consider an expression for the natural frequency of the system, given by:

$$\omega_0 = 2\pi f_0 = \sqrt{\frac{k_{eq}}{m_{eq}}} = \sqrt{\frac{L_k^2 k}{L_1^2 M_{mag} + L_M^2 M + L_{CG2x}^2 M_2 + I_2 + I_M}} \tag{2.17}$$

The above expression allows to determine the natural frequency as function of the moving mass position.

To obtain a general solution the natural frequency and the optimal average power (2.13) can be written in terms of dimensionless parameters, thus:

$$\Omega_0 = \frac{2\pi f_0}{\sqrt{\frac{S}{M_{mag}}}} = \sqrt{\frac{1}{1 + \rho(l_m^2 + i_M) + \delta(l_{cg2x}^2 + i_2)}} \tag{2.18}$$

$$P^*(l_m, \rho, \xi) = \frac{P_L(R_L^*)}{\frac{1}{8} M_{mag}^2 \max(\ddot{y}_1)^2 / 2\zeta\sqrt{SM_{mag}}} = \frac{(1+\rho l_m+\delta l_{cg2x})^2}{\sqrt{1+\rho(l_m^2+i_M)+\delta(l_{cg2x}^2+i_2)}\left(1+\xi\sqrt{1+\rho(l_m^2+i_M)+\delta(l_{cg2x}^2+i_2)}\right)} \tag{2.19}$$

Where,

$$S = kl_k^2 \;\; l_k = \frac{L_k}{L_1} \;\; l_m = \frac{L_M}{L_1} \;\; l_{cg2x} = \frac{L_{cg2x}}{L_1} \;\; \rho = \frac{M}{M_{mag}} \;\; \delta = \frac{M_2}{M_{mag}} \;\; i_M = \frac{I_M}{ML_1^2}$$

$$i_2 = \frac{I_2}{M_2 L_1^2} \;\; \xi = \frac{2\zeta\sqrt{SM_{mag}}}{K_\phi^2/R_{coil}} \tag{2.20}$$

Here S can be regarded as a measure of the rigidity of the system and ρ is the ratio between the moving mass and the mass of the magnet. These two parameters are the main tuning variables of the previously mentioned trade-off.

The dimensionless natural frequency (2.18) and optimal average power (2.19) are shown in Figure 2-5 for different values of ρ and typical values for $l_{cg2x}, \delta, i_M, i_2$ & ξ.

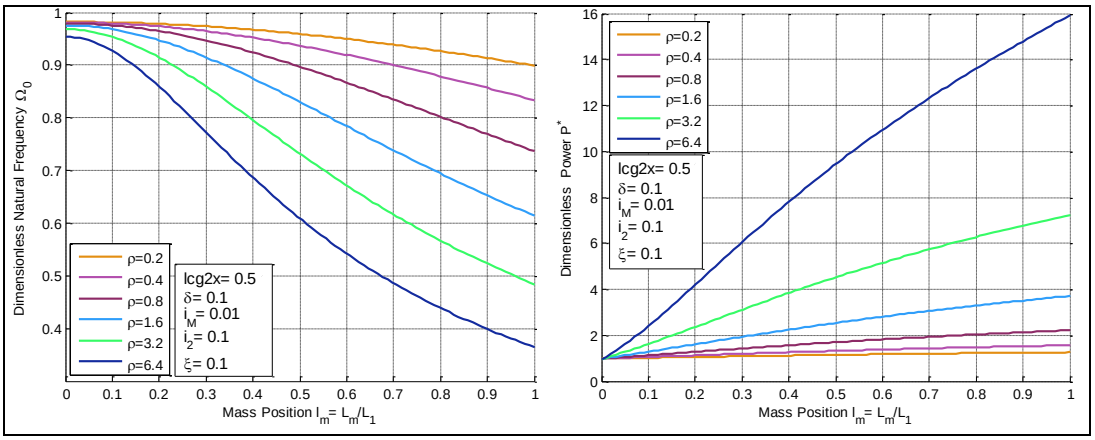

Figure 2-5: Dimensionless natural frequency (left) and maximum average power (right) for different values of ρ, at different positions of the tuning mass.

Figure 2-5 shows that higher values of ρ gives a higher range of frequencies and higher rates of power extracted, since this parameter increases the effective mass of the system. On the other hand moving the position of mass M changes the power extracted for the same reason.

Next, to study the effect of S, Figure 2-6 shows the curve l_m v/s f_0 obtained from (2.18) and the power expression $P_L(R_L^*)$ normalized by the squared value of max($\ddot{y}_1$):

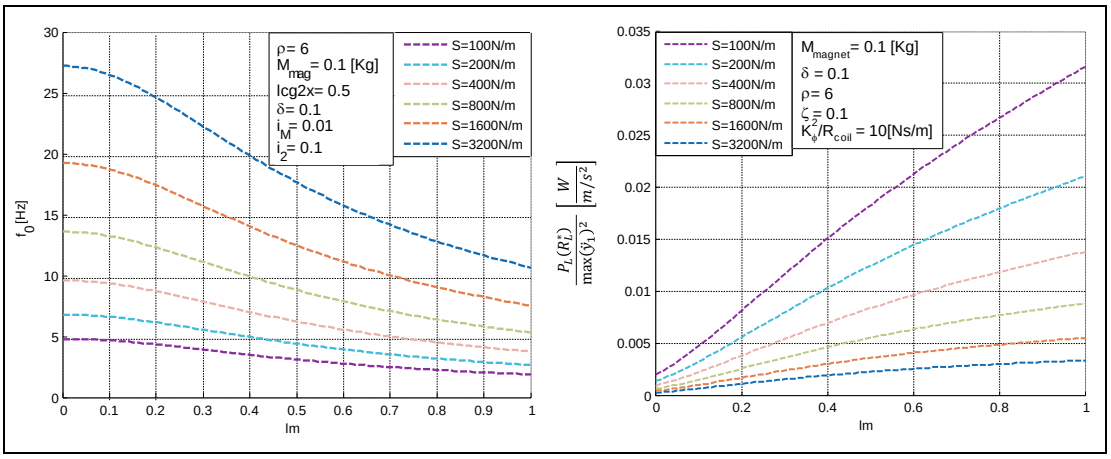

Figure 2-6: Natural frequency (left) and normalized maximum average power (right) for different values of S, at different positions of the tuning mass.

Thus, according to Figure 2-6, modifying the value of S allows the designer to choose the working frequency. However increasing the value of S has a negative effect on the output average power

2.4.3. Geometric Restrictions

An important and obvious restriction for the magnet oscillation is that it should not exceed the physical limits of the device. This consideration should be done for both the equilibrium position θ_0 and the maximum oscillation angle ϑ_{max}.

From the analytical solution of (2.1), the maximum amplitude of oscillation at resonance is given by:

$$\vartheta_{max} = \frac{M_{mag}\max(\ddot{y}_1)}{2L_1 S}\frac{\left(1+\rho l_m+\delta l_{cg2x}\right)}{\left(\zeta+\dfrac{K_\phi^2 L_1^2}{2\sqrt{k_{eq}m_{eq}}(R_{coil}+R_L^*)}\right)} \tag{2.21}$$

Also, the equilibrium position of the horizontal pendulum can be written as function of dimensionless parameters that constitutes the design space: the position of the spring l_k, the position of the mass l_m and the normalized height of the pivot point σ.

$$\theta_0(l_k, l_m, \sigma) = \frac{M_{mag} g}{S L_1}\left(1 + \rho l_m + \delta l_{cg2x}\right) + \frac{L_7}{2L_1}\frac{(2\sigma - 1)}{l_k} \quad ; \quad \sigma = \frac{L_5}{L_7} \qquad (2.22)$$

The geometric restrictions have to ensure that the pendulum will have an equilibrium position that does not strike against the physical limits of the device for both static position and when it reaches ϑ_{max}.

These restrictions are easily obtained by trigonometric relations for the horizontal pendulum, and using an expression for the position of the magnet relative to the base of the device (2.16).

Regarding the design of the proposed harvester, and once S and ρ are fixed, the only parameters that can be used to select a suitable equilibrium position are (σ, l_k, l_m).

Following, the position of the mass at its extremes (i.e. l_m=0 and $l_m = 1$) will make these restrictions active, which eliminates l_m from the design space.

Finally, intersecting the restrictions and applying extremes values for l_m gives a set of inequalities for (σ, l_k). Since the objective is to obtain values that meet these restrictions, is enough to evaluate (σ, l_k) in its entire domain ($[0,1] \times [0,1]$) to obtain a suitable combination.

The following set of inequalities was obtained according to the above discussion, thus giving the reader a sense of the complexity involved in the optimal design using the mathematical model of the device.

$$\vartheta_{max} - \sin^{-1}\big(2\beta(1-\sigma)\big) < \theta_0(l_k, 0, \sigma) \tag{2.23}$$

$$\theta_0(l_k, 1, \sigma) < \tan^{-1}\left(\frac{\beta\big(\sigma - \gamma\sqrt{\beta^2\gamma^2 - \beta^2\epsilon^2 + 2\beta^2\epsilon\sigma - 2\beta^2\epsilon\tau - \beta^2\sigma^2 + 2\beta^2\sigma\tau - \beta^2\tau^2 + 1} - \epsilon - \tau\big)}{\beta^2\gamma^2 + 1}\right) \tag{2.24}$$

$$\theta_0(l_k, 1, \sigma) < \tan^{-1}\left(\frac{\cos(\vartheta_{max})\,\beta\gamma - \beta\gamma + \sin(\vartheta_{max})}{\sin(\vartheta_{max})\,\beta\gamma + 1 - \cos(\vartheta_{max})}\right) \tag{2.25}$$

$$\tau \le \frac{y_{mag}^{base}\big(\theta_0(l_k, 1, \sigma)\big)}{L_7} \tag{2.26}$$

$$\frac{y_{mag}^{base}\big(\theta_0(l_k, 1, \sigma)\big)}{L_7} \le \frac{y_{mag}^{base}\big(-\sin^{-1}\big(2\beta(1-\sigma)\big)\big)}{L_7} \tag{2.27}$$

Where,

$$\alpha = \frac{M_{mag}g}{SL_1} \quad ; \quad \beta = \frac{L_7}{L_1} \quad ; \quad \gamma = \frac{L_2}{L_7} \quad ; \quad \epsilon = \frac{L_3}{L_7} + \frac{L_4}{L_7} + \frac{h_{mag}}{2L_7}$$

$$\tau = \begin{cases} \dfrac{h_{coil}}{L_7}, h_{coil} \ge h_{mag} \\ \dfrac{h_{mag} + h_{coil}}{2L_7}, h_{coil} < h_{mag} \end{cases} \quad ; \quad \frac{y_{mag}^{base}(\theta)}{L_7} = \sigma - \frac{\sin(\theta)}{\beta} - \gamma\cos(\theta) - \epsilon \tag{2.28}$$

2.5. Experimental Results and Validation

An experimental prototype was built (see Figure 2-7) to validate the model of the harvester. The linear motion of the moving mass is controlled by a DC motor driving a power screw. The position of the moving mass is sensed by a potentiometer. A radial ball bearing allows pivoting of the horizontal beam. The structure is mainly made of aluminum profiles.

The inertia properties and center of gravity locations were computed using a 3D Cad software. The relevant physical properties of the device are given in Table 2-1.

Table 2-1: Physical properties of the prototype

Symbol	Description	Value
L_1	Length of pendulum	337 [mm]
L_7	Height from base to top	230 [mm]
M_{mag}	Mass of magnet	170 $[g]$
M	Moving mass	514 [g]
M_2	Mass of the pendulum	870 $[g]$
I_2	Rotational inertia of body 2	$27 \cdot 10^{-4}$ [Kg m^2]
I_m	Rotational inertia of moving mass	$1.05 \cdot 10^{-4}$[Kg m^2]
L_{CG2x}	Distance to center of gravity for body 2	137 [mm]

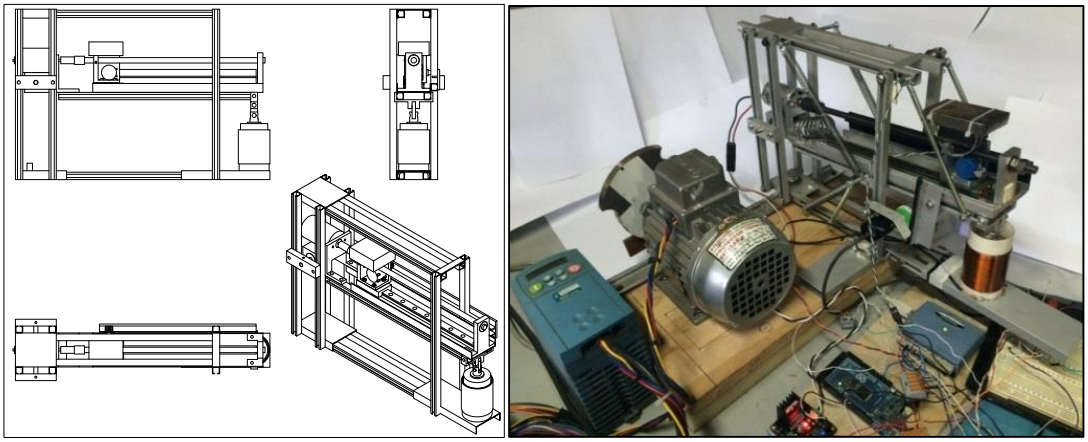

Figure 2-7: 3D model of the device (left) and experimental setup (right).

2.5.1. Experimental Validation of Induced Voltage ε_{in}

Experimental validation of the induced voltage ε_{in} was performed in a pivoted arm that holds the magnet at the opposite end by means of helical tension springs, as seen in Figure 2-7.

The position of magnet was obtained by means of a calibrated rotary encoder. A data acquisition system was used to read the voltage output. The magnet was left to oscillate freely from an initial position. The speed of the magnet was estimated by processing offline the rotary encoder signal.

Thus, knowing the position, speed of the magnet and the curve $K_\phi(z)$, voltage output can be built. The experimental results were compared to those obtained mathematically using expressions (2.1) & (2.2) according to parameters given in Table 2-2, where approximated model for K_ϕ is shown in Figure 2-8.

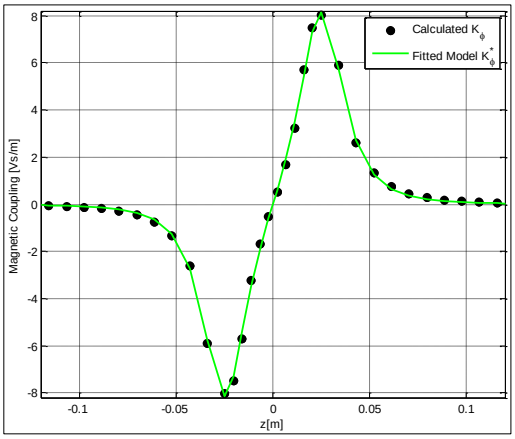

Figure 2-8: Identified model for K_ϕ used in the experimental validation of ε_{in}.

Table 2-2 Parameters of coil and magnet used in the experimental validation

Symbol	**Quantity**	**Value**
h_{magnet}	Magnet height	$20 \cdot 10^{-3}$ m
r_{magnet}	Magnet radius	$20 \cdot 10^{-3}$ m
B_r	Remanence of N35 Neodymium magnet	1.17 T
N_z	Turns per layer	135
N_r	Number of layers	4
d	Wire thickness	$0.37 \cdot 10^{-3}$ m
R_{coil}^{in}	Air gap	$1 \cdot 10^{-3}$ m

Both theoretical and experimental curves are shown in Figure 2-9, where also magnet position relative to the coil is shown.

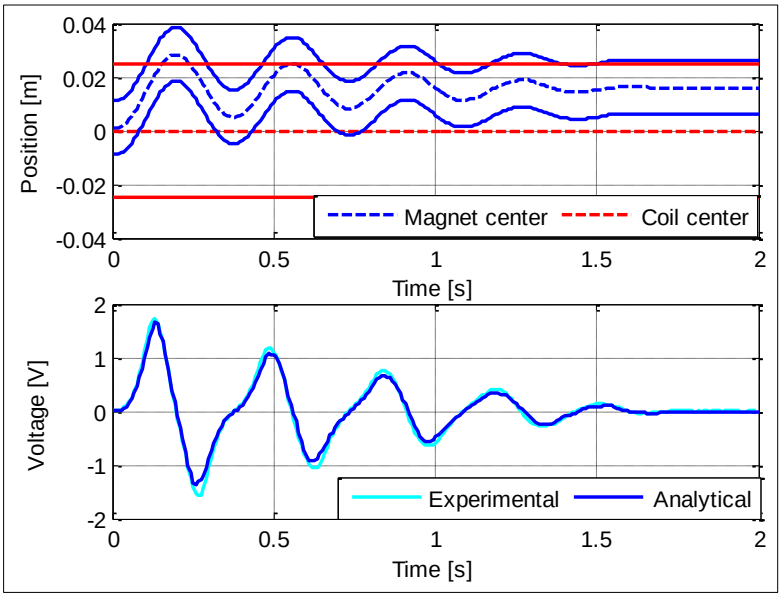

Figure 2-9: Graphic comparison of the experimental induced voltage vs the one calculated by the model.

It can be seen that the similitude of both the experimental and theoretical results is quite satisfactory

In Figure 2-9, the square mean error normalized to the maximum amplitude between experimental voltage (V_E) and analytical voltage (ε_{in}) is 2.28 % when computed in the time interval between 2s to 4s.

It can be observed from Figure 2-8 that the maximum magnetic flux occurs when the magnet center point passes through the rim of the coil, hence the optimum equilibrium position for the coil-magnet assembly is given by

$$z_0^* = \begin{cases} \frac{h_{coil}}{2}, h_{coil} \geq h_{mag} \\ \frac{h_{mag}}{2}, h_{coil} < h_{mag} \end{cases} \quad (2.29)$$

2.5.2. Validation of Magnetic Force by Finite Element Method simulation.

In order to validate our method for computing magnetic force (2.5) a finite element simulation was carried out and compared with a numerical simulation of a state space model.

A magnet supported by a spring oscillates inside a copper coil which is connected in series to an electric resistive load. Loses due to air friction are neglected. The base is subject to a sinusoidal change in its position rather than a sinusoidal acceleration as seen in (2.30). Hence the dynamic equations for such a system are:

$$\dot{z}_{mag} = v_{mag}$$

$$\dot{v}_{mag} = \frac{1}{m_{magnet}}\left(k\left(\left(z_{base}(t) - z_{base}^{eq}\right) - \left(z_{mag} - z_{mag}^{eq}\right)\right) - IK_{\phi}\left(z_{mag}\right)\right) \tag{2.30}$$

$$\dot{I} = \frac{1}{L}\left(K_{\phi}\left(z_{mag}\right)v_{mag} - I\left(R_L^{\Omega} + R_{coil}^{\Omega}\right)\right)$$

The above model was simulated in MATLAB with parameters given in Table 2-3. MATLAB command *ode15s* was used to integrate trough time this system of differential equations.

The inductance of the analytical model as well as the coil resistance was estimated using classical approximations such as given in (Wheeler, 1928).

Magnetic coupling K_{ϕ} is computed with equation (2.2) for a set of fixed magnet positions and intermediate results are interpolated by approximating according to equation (2.3). Figure 2-10 shows the result of the fitted curve.

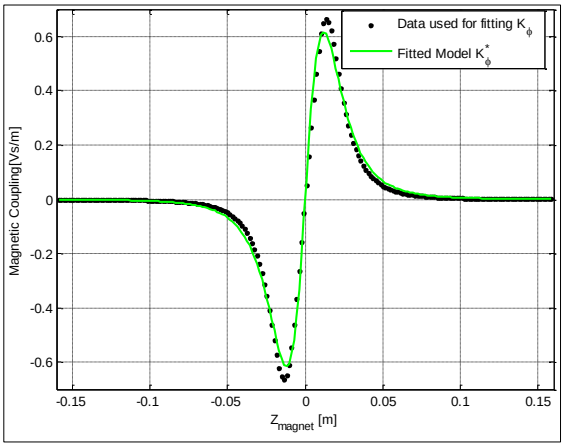

Figure 2-10: Fitted model for K_ϕ used in the finite element validation for electromagnetic force.

Next, a simulation was carried with the COMSOL Multiphysics software using parameters given in Table 2-3 below. The magnetic coupling, voltage output, coil current and magnetic force are computed at every time interval. The magnetic force is computed by integrating Lorentz´ force for the entire length of the coil.

Table 2-3 Parameters used in the finite elements validation

Symbol	**Quantity**	**Value**
h_{magnet}	Magnet height	$25 \cdot 10^{-3}$[m]
R	Magnet radius	$12.5 \cdot 10^{-3}$ [m]
B_r	Remanence of magnet	1.17 [T]
N_z	Turns per layer	10
N_r	Number of layers	5
d	Wire thickness	$1 \cdot 10^{-3}$[m]
$R_{coil}^{in} - R$	Air gap	$5 \cdot 10^{-3}$ [m]
L	Coil Inductance	$2.8 \cdot 10^{-5}$ [H]
ρ_{copper}	Copper resistivity	$1.71 \cdot 10^{-8}$[Ωm]
R_{coil}^{Ω}	Load	0.13 [Ω]
R_L^{Ω}	Load	1000 [Ω]
m_{magnet}	Magnet mass	0.0834 [Kg]
f	Excitation frequency	10 [Hz]
k	Spring constant	658.8[N/m]
t_f	Simulation time	0.25 [s]

dt	Time step for integration	0.00125 [s]
z_{base}^{eq}	Equilibrium position of base	0.1 [m]
z_{magnet}^{eq}	Equilibrium position of magnet	0 [m]
$z_{base}(t)$	Moving base oscillation	$h_{magnet}\ \sin(2\pi f\, t)/2 - 0.1$

The mesh in the simulation is time variant (Figure 2-11) adapting to the motion determined by equations (2.30).

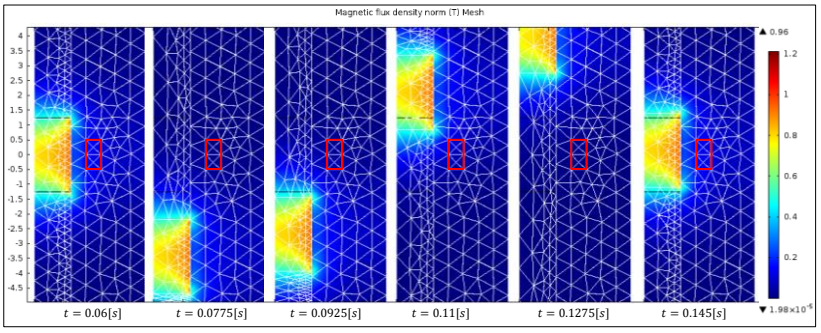

Figure 2-11: Moving mesh used in COMSOL. The color indicates the norm of the magnetic flux density produced by the magnet. The red square symbolizes the position of the coil.

Figure 2-12 shows results of FEM computed values obtained with COMSOL compared to results of numerical simulations in MATLAB for the magnetic force.

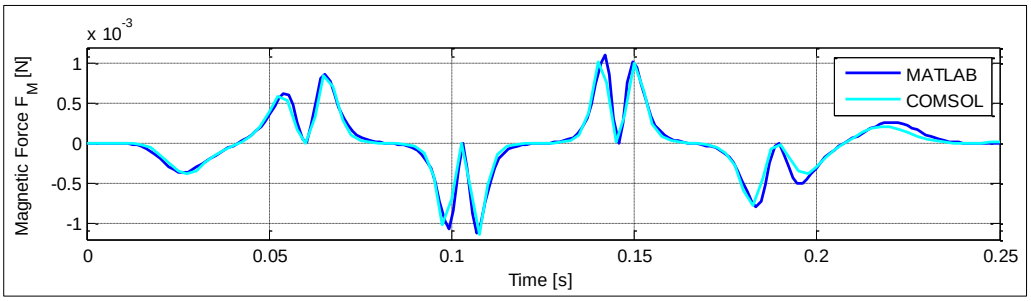

Figure 2-12: Results of the validation for the magnetic force using finite elements software.

The mean square error in the magnetic force computed by MATLAB and COMSOL is 3.29% in the time interval shown in Figure 2-12.

Simulation time is staggeringly different in both approaches. While the numerical approach proposed by the authors took 38 seconds in MATLAB environment, the FEM simulation took over 30 minutes in computers with similar processing power. Note that MATLAB code was interpreted at execution time, so a compiled version would take even less time.

Given the high accuracy and low computation time of the numerical modeling approach here suggested by the authors it is clearly convenient for design purposes, where a large number of simulation runs are necessary while searching for an optimum or near optimum design.

2.5.3. Experimental verification of the natural frequency and critical damping factor.

The natural frequency for different positions of the moving mass was obtained using an accelerometer to register oscillations when the system was allowed to oscillate from a given initial starting condition. A behavior of the form given in (2.31) was observed.

$$Me^{(-\zeta\omega_0 t)}\sin\left(\omega_0\sqrt{1-\zeta^2}t+\varphi\right) \tag{2.31}$$

Least squared fitting was carried out to obtain the critical damping factor from (2.31). The fitted model is compared with free oscillation data in Figure 2-13 (a).

Natural frequency is obtained from the Fast Fourier Transform (FFT) of the free oscillation response, as seen in Figure 2-13 (b). Sample rate was 1000Hz, FFT was applied in the range 0Hz to 10Hz, for 2^{14}=16384 samples, which gives a resolution of $\Delta f = \frac{1000[Hz]}{2^{13}} = 0.122\ [Hz]$. Peak value observed corresponds to the damped natural frequency. The testing parameters are given in Table 2-4.

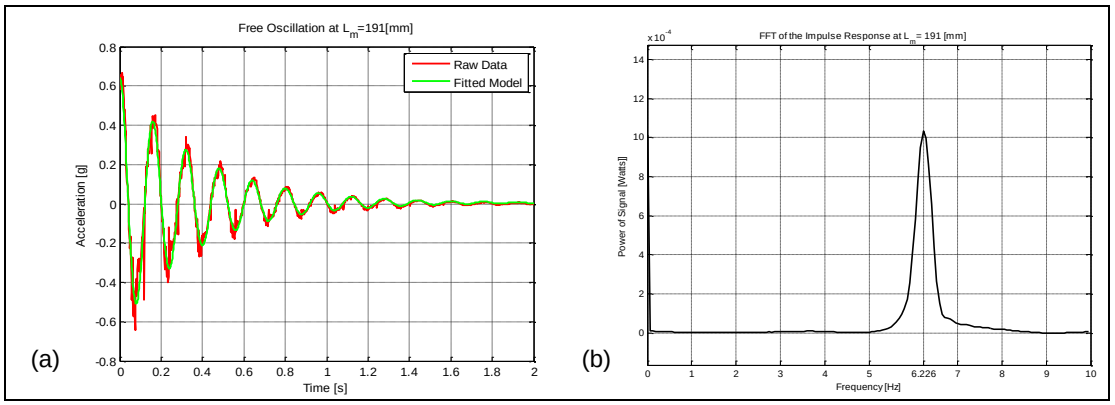

Figure 2-13: (a) Free oscillation used to determine natural frequency and to calculate the critical damping factor. (b) FFT of the free oscillation data.

Table 2-4 Physical properties of the prototype used for damping factor calculation

Symbol	Description	Value
L_m	Position of tuning mass	191 [mm]
L_k	Position of springs	264[mm]
k	Equivalent Stiffness	1274 [N/m]
σ	Ratio L_5/L_7, where $L_5$is the height of the pivot point	0.174

The computed natural frequency is $6.22[Hz]$ and critical damping factor is 6.75%

2.5.4. Equivalent Stiffness and Equilibrium Position

Knowing the natural frequency we can obtain the equivalent spring constant of the system given by the following expression (2.32),

$$k(f_0) = \frac{(2\pi f_0)^2\left(L_1^2 M_{mag} + L_M^2 M + L_{CG2x}^2 M_2 + I_2 + I_M\right)}{L_k^2} \tag{2.32}$$

Now, by virtue of (2.9), the equilibrium position (or resting position) can be obtained. Figure 2-14 shows the computed value of natural frequency and equilibrium position versus the moving mass position.

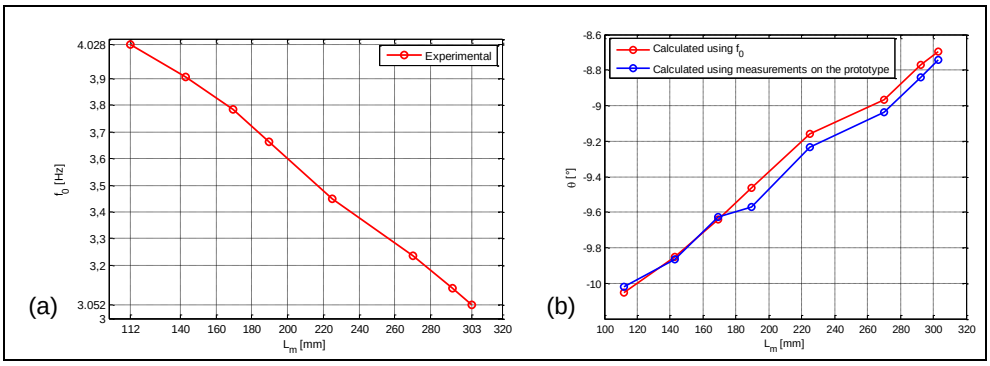

Figure 2-14: (a) Measured natural frequency. (b) Calculated equilibrium angle compared with the measured in the prototype.

Table 2-5 Properties of the prototype used for validation of equivalent stiffness and equilibrium position

Symbol	Quantity	Value
k	Mean equivalent stiffness	1564 $[N/m]$
L_k	Position of springs	139 [mm]
σ	Ratio L_5/L_7, where $L_5$is the height of the pivot point	0.345

Table 2-5 shows the parameters used in this section. The stiffness of the system changes slightly when the position of the mass L_M is modified because the extension of the helical springs changes too. This moves the spring from its linear operational zone. Nonetheless, the model can predict the equilibrium angle if the stiffness is calculated for the initial and the final position off the mass and then a linear fitted is used.

2.5.5. Output Voltage and Power

With parameters of Table 2-6 the time response of the system (2.10) was simulated for different values of the electric load R_{load}in order to compare the theoretical average output power (2.13) and the RMS voltage with experimental measurements done in the prototype with the same parameters. Measurements were done at 500Hz of sampling frequency.

Theoretical average output power was calculated using the following relation that comes from the derived expressions of section 2.3.3:

$$\bar{P} = \frac{1}{T}\int_0^T I(t)v_{load}(t)\,dt = c_L \frac{\max\left(F_e(t)\right)^2}{2c_{eq}^2} \tag{2.33}$$

Where c_L is the damping produced by the dissipation of energy in R_{load}:

$$c_L = R_{load}\frac{K_\phi^2}{(R_{coil}+R_{load})^2}L_1^2 \tag{2.34}$$

Figure 2-15 shows the comparison along with the theoretical maximum average output power and the open circuit voltage.

Table 2-6: Configuration used to validate voltage and power expressions

Symbol	Quantity	Value
L_{m_0}	Position of mass	197 [mm]
f_0	Natural frequency at L_{m_0}	6.22 [Hz]
k	Mean equivalent stiffness	1529 $[N/m]$
L_k	Position of springs	241 [mm]
l_k	Normalized Position of springs L_k/L_1	0.717
σ	Ratio L_5/L_7	0.1695
K_ϕ^{max}	Maximum value of K_ϕ used to calculate R_L^*	8.153 $[Vs/m]$
R_{coil}^{real}	Measured coil resistance in the prototype	16 [Ω]
R_{coil}^{model}	Coil resistance given by the model	11.7 [Ω]
$R_L^{real^*}$	Measured optimal load	39.7 [Ω]
R_L^*	Calculated optimal load	36.16[Ω]
$\ddot{y}_1$	Base acceleration	$0.13gcos(2\pi f_0 t)$ $[m/s^2]$
ζ	Critical damping factor	6.75%
$P_L^*(R_L^*)$	Theoretical maximum average output power	0.0344 $[W]$

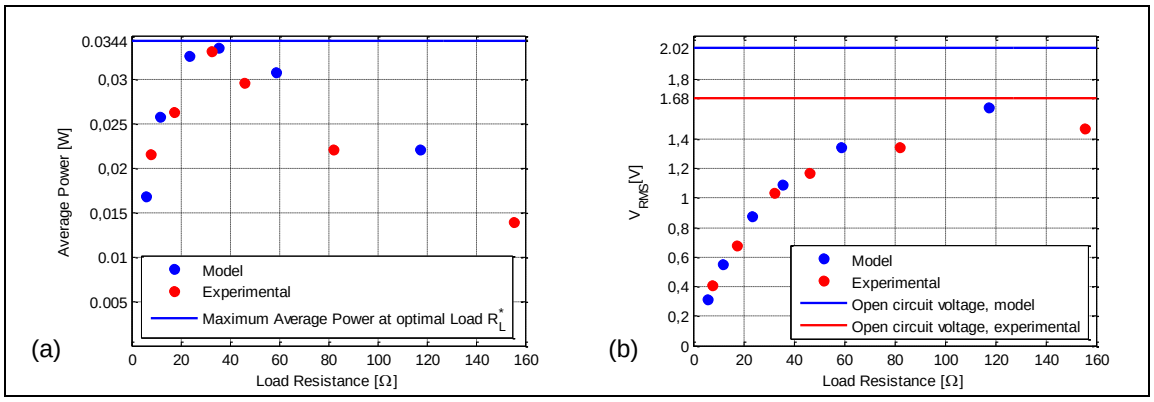

Figure 2-15: Experimental validation of the model for (a) average power $\bar{P}$ and (b) RMS voltage.

A good agreement between the experimental results and the given expressions for power and output voltage are shown in Figure 2-15.

2.5.6. Power vs Frequency comparison

The power extracted, assuming optimal load resistance, for the whole range of frequencies of the prototype was simulated with the parameters of Table 2-6 for 3 cases: with fixed f_0, tunable f_0 without adjustment of the relative position of magnet and coil (z_{mag}) and for the proposed scheme: tunable f_0 with adjustment of z_{mag}.

Additionally the response for the same three cases but for an improved configuration was simulated.

The improved configuration was obtained as a result of the analysis done in Section 2.4.2 where was concluded that increasing the value of the ratio $\rho = M/M_{mag}$ allows for an increased frequency range and power. Also, the coil parameters where enhanced, increasing the value of K_ϕ^2/R_{coil} as pointed out in Section 2.3.2. The improved parameters are shown in Table 2-7.

Table 2-7: Improved parameters found using the developed model

Symbol	Description	Value
N_z	Turns per layer	60
N_r	Number of layers	35
$\max(K_\phi)$	Maximum value of magnetic coupling	36.75 [Vs/m]
R_{coil}	Coil resistance	57.65[Ω]
M	Moving mass	1041 [g]
M_2	Mass of the pendulum	455 $[g]$
I_m	Rotational inertia of moving mass from its center of gravity	$21 \cdot 10^{-4}$[Kg m^2]
I_2	Rotational inertia of body 2 from its center of gravity	$23.9 \cdot 10^{-4}$ [Kg m^2]
L_{CG2x}	Distance to center of gravity for body 2	96 [mm]
l_k	Normalized Position of springs L_k/L_1	0.7596
σ	Ratio L_5/L_7	0.3250

The comparison of both configurations for the three cases is shown in Figure 2-16.

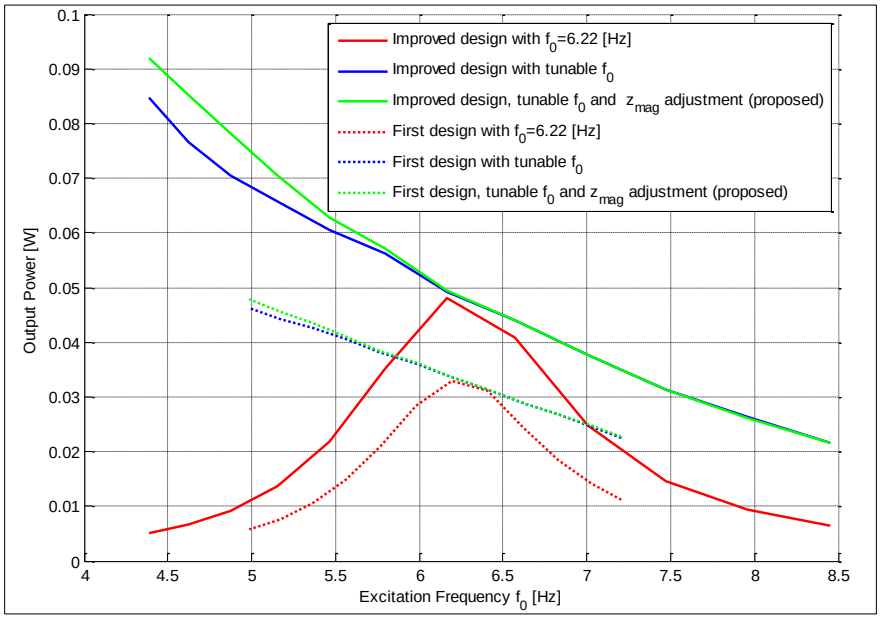

Figure 2-16: Comparison of the response of the proposed scheme with other strategies for the actual configuration and for an improved one.

Figure 2-16 shows that the use of a frequency tuning technique greatly increases the output power, improving the frequency response. Moreover, with the proposed configuration, the output power can be increased even more for certain frequencies ranging from an increase of 0.4% at 6.22[Hz] to 9.8% at 4.39[Hz].
Furthermore, the analysis of the model showed up the critical points to improve the performance of the system, resulting in an increase 48% of the output power at the design frequency $f_0 = 6.22[Hz]$ and the extension of the range of frequencies in 82%.

2.6. Discussion of Results

The energy harvesting configuration discussed in this article has been analyzed previously by other authors (Schaufuss et al., 2011; Zhu et al., 2010), however in this work we have introduced a model with a complete set of validated equations and design considerations to follow for obtaining a near optimal design.

An additional advantage of this model is that it can be simulated using vibration excitation data taken from real machines, in order to obtain a design for a particular application.

The effect of friction is taken into account in the proposed model because in this kind of application it has a great effect in power output and oscillation magnitude.

The prototype configuration analyzed here can be enhanced by adding features such as stoppers, nonlinear springs and others strategies to increase the bandwidth (Zhu et al., 2010). However additional cost and space would be required.

The automatic control system for adjusting the natural frequency of the system must be one of low energy consumption since otherwise the net energy output would be negative. This is a topic that must be addressed and optimized in the further development of this concept.

Previous published works studying similar configurations treat magnetic coupling K_ϕ as a fixed value. However rigorously speaking it is not fixed and its changing value depending on the magnet equilibrium position affects power output. For this reason in the proposed model K_ϕ is computed instantaneously to obtain the output voltage.

However in computing the optimal load resistance, due to the mathematical complexity it is more practical to use the maximum value of K_ϕ, because it was found that the difference resulted negligible.

The proposed configuration increased slightly the prototype power. Nonetheless, this effect would be increased for coil-magnet systems with narrow K_ϕ curves or for designs where the equilibrium position changes significantly when tuning the frequency.

The output power achieved with the prototype, with a suitable power management circuit, is enough to feed some commercially available Wireless Sensor Nodes like the MicaZ+MTS310CB which has an average consumption of $186\ [\mu W]$ while sensing accelerations (Chamanian et al., 2014).

The improved configuration found is far from being the most efficient electromagnetic vibration harvester (Moss et al., 2015) but with the presented model a more efficient prototype can be designed.

The proposed configuration is meant to be used in heavy off road vehicles such as mining trucks or all terrain armored vehicles. In these cases the terrain is very uneven and the speed travel is widely varying, hence the available excitation frequency spectrum is wide. Better performance could achieved with a configuration that is able to adjust its natural frequency periodically as the one presented in this work, but it still require a comparison with broadband strategies.

Other low frequency macro-scale applications could be a wave energy converter, since the natural frequency could be tuned to harvest the energy from an incoming ocean wave.

2.7. Conclusions and Future work

In the present work, modeling, validation and design considerations of energy harvesting device in a horizontal pendulum configuration has been discussed thoroughly. In this context a parametric model apt for design purposes is now available which considers with good degree of accuracy the magnetic coupling at the coil magnet assembly. Also taken into account is the design trade-off between frequency range and magnitude of power extraction. Furthermore, also considered is the optimal load that will instantaneously give the maximum power output.

The parametric model presented here allows to simulate the dynamic response and instantaneous power extraction. Using this model some design considerations are presented to obtain a balanced output in power versus frequency range. In addition geometric restrictions for proper functioning are derived.

A prototype was built and tested, allowing to experimentally validate the model.

From the model was found an optimal resting position of the magnet respect to coil, which is perturbed when tuning the frequency. Moving the coil to keep that optimal position when tuning the frequency allows to obtain an increase in power output.

Future work will consider the formulation of algorithms for maximum power tracking, that is to say the automatic adjustment of the configuration given a user load and available external excitation frequencies.

REFERENCES

Agostinacchio, M., Ciampa, D., & Olita, S. (2013). The vibrations induced by surface irregularities in road pavements - a Matlab approach. *European Transport Research Review*, 1–9. http://doi.org/10.1007/s12544-013-0127-8

Akhtar, F., & Husain, M. (2015). Energy replenishment using renewable and traditional energy resources for sustainable wireless sensor networks : A review. *Renewable and Sustainable Energy Reviews*, *45*, 769–784. http://doi.org/10.1016/j.rser.2015.02.021

Avila Bernal, a. G., & Linares García, L. E. (2012). The modelling of an electromagnetic energy harvesting architecture. *Applied Mathematical Modelling*, *36*(10), 4728–4741. http://doi.org/10.1016/j.apm.2011.12.007

Beeby, S. P., Tudor, M. J., & White, N. M. (2006). Energy harvesting vibration sources for microsystems applications. *Measurement Science and Technology*, *17*(12), R175–R195. http://doi.org/10.1088/0957-0233/17/12/R01

Berdy, D. F., Valentino, D. J., & Peroulis, D. (2014). Design and Optimization of a Magnetically Sprung Block Magnet Vibration Energy Harvester. *Sensors and Actuators A: Physical*. http://doi.org/10.1016/j.sna.2014.06.011

Boisseau, S., Despesse, G., & Seddik, B. A. (2012). Electrostatic Conversion for Vibration Energy Harvesting. In M. Lallart (Ed.), *Small-Scale Energy Harvesting* (pp. 91–134). InTech. http://doi.org/10.5772/51360

Borca-Tasciuc, D.-A., Hella, M., & Kempitiya, A. (2010). Micro-power generators for ambient intelligence applications. *4th International Workshop on Soft Computing Applications*, 19–24. http://doi.org/10.1109/SOFA.2010.5565632

Cepnik, C., Lausecker, R., & Wallrabe, U. (2013). Review on Electrodynamic Energy Harvesters—A Classification Approach. *Micromachines*, *4*(2), 168–196. http://doi.org/10.3390/mi4020168

Cepnik, C., Radler, O., Rosenbaum, S., Ströhla, T., & Wallrabe, U. (2011). Effective optimization of electromagnetic energy harvesters through direct computation of the electromagnetic coupling. *Sensors and Actuators A: Physical*, *167*(2), 416–421. http://doi.org/10.1016/j.sna.2011.01.023

Chamanian, S., Baghaee, S., Ulusan, H., Zorlu, Ö., Külah, H., & Uysal-Biyikoglu, E. (2014). Powering-up Wireless Sensor Nodes Utilizing Rechargeable Batteries and an Electromagnetic Vibration Energy Harvesting System. *Energies*, *7*(10), 6323–6339. http://doi.org/10.3390/en7106323

Davino, D., Giustiniani, A., & Visone, C. (2012). Magnetoelastic Energy Harvesting: Modeling and Experiments. In Giovanni Berselli (Ed.), *Smart Actuation and Sensing Systems-Recent Advances and*. http://doi.org/10.5772/50892

Eichhorn, C., Tchagsim, R., Wilhelm, N., & Woias, P. (2011). A smart and self-sufficient frequency tunable vibration energy harvester. *Journal of Micromechanics and Microengineering*, *104003*. http://doi.org/10.1088/0960-1317/21/10/104003

Gagliardi, J., & Utt, W. K. (1993). *Vibration Enviromental Testing for Large Haulage Trucks*. *Report of Investigations* (Vol. 9483). United States Department of the Interior, Bureau of Mines. Retrieved from http://stacks.cdc.gov/view/cdc/10278

Galchev, T., Kim, H., & Najafi, K. (2011). Micro power generator for harvesting low-frequency and nonperiodic vibrations. *Journal of Microelectromechanical Systems*, *20*(4), 852–866. http://doi.org/10.1109/JMEMS.2011.2160045

Hawley, J. (2012). Modeling a cylindrical permanent magnet with a surface charge of magnetic monopoles. Retrieved from http://www.jimhawley.ca/downloads/Permanent_Magnet_With_Magnetic_Monopole_Surface_Charge.pdf

Howard, R. A., Member, S., Xiao, Y., & Pekarek, S. D. (2013). Modeling and Design of Air-Core Tubular Linear Electric Drives. *IEEE Transactions on Energy Conversion*, *28*(4), 793–804.

Jiang, X., Li, Y., & Li, J. (2013). Design of a novel linear permanent magnet vibration energy harvester. *2013 IEEE/ASME International Conference on Advanced Intelligent Mechatronics*, 1090–1095. http://doi.org/10.1109/AIM.2013.6584239

Jung, H. J., Park, J., & Kim, I. H. (2012). Investigation of applicability of electromagnetic energy harvesting system to inclined stay cable under wind load. *IEEE Transactions on Magnetics*, *48*(11), 3478–3481. http://doi.org/10.1109/TMAG.2012.2202889

Jung, H.-J., Kim, I.-H., Min, D. Y., Sim, S.-H., & Koo, J.-H. (2013). A hybrid electromagnetic energy harvesting device for low frequency vibration. In *SPIE, Active and Passive Smart Structures and Integrated Systems* (Vol. 8688, p. 86881I). San Diego, California: SPIE. http://doi.org/10.1117/12.2010014

Khaligh, A., Member, S., Zeng, P., Member, S., Zheng, C., & Member, S. (2010). Kinetic Energy Harvesting Using Piezoelectric and Electromagnetic Technologies — State of the Art. *IEEE Transactions on Industrial Electronics*, *57*(3), 850–860.

Kim, I.-H., Jang, S.-J., & Jung, H.-J. (2013). Performance enhancement of a rotational energy harvester utilizing wind-induced vibration of an inclined stay cable. *Smart Materials and Structures*, *22*(7), 075004. http://doi.org/10.1088/0964-1726/22/7/075004

Li, H., Tian, C., & Deng, Z. D. (2014). Energy harvesting from low frequency applications using piezoelectric materials. *Applied Physics Reviews*, *1*(4), 041301. http://doi.org/10.1063/1.4900845

Liu, H., Qian, Y., & Lee, C. (2013). A multi-frequency vibration-based MEMS electromagnetic energy harvesting device. *Sensors and Actuators A: Physical*, *204*, 37–43. http://doi.org/10.1016/j.sna.2013.09.015

Liu, X. (2012). An Electromagnetic Energy Harvester for Powering Consumer Electronics. *All Theses*. Paper 1415. Retrieved from http://tigerprints.clemson.edu/all_theses/1415/

Mathúna, C. O., O'Donnell, T., Martinez-Catala, R. V, Rohan, J., & O'Flynn, B. (2008). Energy scavenging for long-term deployable wireless sensor networks. *Talanta*, *75*(3), 613–23. http://doi.org/10.1016/j.talanta.2007.12.021

Mccarthy, K., Bash, M., Pekarek, S., Krause, P. C., & Lafayette, W. (2008). Design of an air-core linear generator drive for energy harvest applications. In *Applied Power Electronics Conference and Exposition, 2008. APEC 2008.* (pp. 1832–1838).

Mitcheson, P., Green, T. C., M.Yeatman, E., & S., H. A. (2004). Architectures For Vibration Driven Micropower Generators. *Journal of Microelectromechanic System*, *13*(3), 429–440.

Moss, S. D., Payne, O. R., Hart, G. a., & Ung, C. (2015). Scaling and power density metrics of electromagnetic vibration energy harvesting devices. *Smart Materials and Structures*, *24*(2), 023001. http://doi.org/10.1117/12.2048061

Munaz, A., Lee, B.-C., & Chung, G.-S. (2013). A study of an electromagnetic energy harvester using multi-pole magnet. *Sensors and Actuators A: Physical*, *201*, 134–140. http://doi.org/10.1016/j.sna.2013.07.003

Patel, P., & Khamesee, M. B. (2013). Electromagnetic micro energy harvester for human locomotion. *Microsystem Technologies*, *19*(9-10), 1357–1363. http://doi.org/10.1007/s00542-013-1820-1

Peralta, M., Costa-Krämer, J. L., Medina, E., & Donoso, A. (2014). Analysis and fabrication steps for a 3D-pyramidal high density coil electromagnetic micro-generator for energy harvesting applications. *Sensors and Actuators A: Physical*, *205*, 103–110. http://doi.org/10.1016/j.sna.2013.10.012

Ravaud, R., Lemarquand, G., Babic, S., Lemarquand, V., & Akyel, C. (2010). Cylindrical Magnets and Coils: Fields, Forces, and Inductances. *IEEE Transactions on Magnetics*, *46*(9), 3585–3590. http://doi.org/10.1109/TMAG.2010.2049026

Reza-Kashyzadeh, K., Ostad-Ahmad-Ghorabi, M. J., & Arghavan, A. (2013). Study Effects of Vehicle Velocity on a Road Surface Roughness Simulation. *Applied Mechanics and Materials*, *372*, 650–656. http://doi.org/10.4028/www.scientific.net/AMM.372.650

Robertson, W., Cazzolato, B., & Zander, a. (2011). A Simplified Force Equation for Coaxial Cylindrical Magnets and Thin Coils. *IEEE Transactions on Magnetics*, *47*(8), 2045–2049. http://doi.org/10.1109/TMAG.2011.2129524

Saha, C. R., O'Donnell, T., Loder, H., Beeby, S., & Tudor, J. (2006). Optimization of an Electromagnetic Energy Harvesting Device. *IEEE Transactions on Magnetics*, *42*(10), 3509–3511. http://doi.org/10.1109/TMAG.2006.879447

Schaufuss, J., & Mehner, J. (2012). MEMS design for an efficient electrostatic energy harvester combined with components of precision mechanics. *International Multi-Conference on Systems, Signals and Devices, SSD 2012 - Summary Proceedings*, *2*(2). http://doi.org/10.1109/SSD.2012.6197965

Schaufuss, J., Scheibner, D., & Mehner, J. (2011). New approach of frequency tuning for kinetic energy harvesters. *Sensors and Actuators A: Physical*, *171*(2), 352–360. http://doi.org/10.1016/j.sna.2011.07.022

Spreemann, D., Folkmer, B., Maurath, D., & Manoli, Y. (2006). Tunable transducer for low frequency vibrational energy scavenging. In *Proceedings of 20th Eurosensors Conference*. Göteborg, Sweden.

Spreemann, D., & Manoli, Y. (2012). *Electromagnetic Vibration Energy Harvesting Devices*. *Media*. http://doi.org/10.1007/978-94-007-2944-5

Stephen, N. G. (2006). On energy harvesting from ambient vibration. *Journal of Sound and Vibration*, *293*(1-2), 409–425. http://doi.org/10.1016/j.jsv.2005.10.003

Tang, L., Yang, Y., & Soh, C. K. (2010). Toward Broadband Vibration-based Energy Harvesting. *Journal of Intelligent Material Systems and Structures*, *21*(18), 1867–1897. http://doi.org/10.1177/1045389X10390249

Wang, L., & Yuan, F. G. (2008). Vibration energy harvesting by magnetostrictive material. *Smart Materials and Structures*, *17*(4), 045009. http://doi.org/10.1088/0964-1726/17/4/045009

Weddell, A. S., Zhu, D., Merrett, G. V, & Beeby, S. P. (2012). A practical self-powered sensor system with a tunable vibration energy harvester. In *PowerMEMS* (pp. 4–7).

Wheeler, H. a. (1928). Simple Inductance Formulas for Radio Coils. *Proceedings of the Institute of Radio Engineers*, *16*(10), 1398–1400. http://doi.org/10.1109/JRPROC.1928.221309

Williams, C. B., Shearwood, C., Harradine, M. A., Mellor, P. H., Birch, T. S., & Yates, R. B. (2001). Development of an electromagnetic micro-generator. *Circuits, Devices and Systems, IEEE Proceedings*, *148*(6), 337–342.

Williams, C. B., & Yates, R. B. (1995). Analysis of a micro-electric generator for microsystems. In *The 8th International Conference on Solid-State Sensors and Actuators, and Eurosensors IX* (Vol. 44).

Xiao, H., & Wang, X. (2014). A review of Piezoelectric Vibration Energy Harvesting Techniques. *International Review of Mechanical Engineering2*. http://doi.org/10.4028/www.scientific.net/AMM.44-47.2945

Ylli, K., Hoffmann, D., Willmann, A., Becker, P., Folkmer, B., & Manoli, Y. (2015). Energy harvesting from human motion : exploiting swing and shock excitations. *Smart Materials and Structures*, *24*(2), 25029. http://doi.org/10.1088/0964-1726/24/2/025029

Zahid Kausar, A. S. M., Reza, A. W., Saleh, M. U., & Ramiah, H. (2014). Energizing wireless sensor networks by energy harvesting systems: Scopes, challenges and approaches. *Renewable and Sustainable Energy Reviews*, *38*, 973–989. http://doi.org/10.1016/j.rser.2014.07.035

Zeng, P., & Khaligh, A. (2013). A Permanent-Magnet Linear Motion Driven Kinetic Energy Harvester. *IEEE Transactions on Industrial Electronics*, *60*(12), 5737–5746. http://doi.org/10.1109/TIE.2012.2229674

Zhou, J., Goodall, R., Ren, L., & Zhang, H. (2009). Influences of car body vertical flexibility on ride quality of passenger railway vehicles. *Proceedings of the Institution of Mechanical Engineers, Part F: Journal of Rail and Rapid Transit*, *223*(5), 461–471. http://doi.org/10.1243/09544097JRRT272

Zhu, D., Tudor, M. J., & Beeby, S. P. (2010). Strategies for increasing the operating frequency range of vibration energy harvesters: a review. *Measurement Science and Technology*, *21*(2), 022001. http://doi.org/10.1088/0957-0233/21/2/022001

Zuo, L., & Tang, X. (2013). Large-scale vibration energy harvesting. *Journal of Intelligent Material Systems and Structures*, *24*(11), 1405–1430. http://doi.org/10.1177/1045389X13486707

Zuo, L., & Zhang, P.-S. (2013). Energy Harvesting, Ride Comfort, and Road Handling of Regenerative Vehicle Suspensions. *Journal of Vibration and Acoustics*, *135*(1), 011002. http://doi.org/10.1115/1.4007562

APPENDIX

A. DERIVATION OF THE ELECTROMAGNETIC COUPLING COEFFICIENT EXPRESSION

In order to obtain the induced voltage produced by a changing magnetic field passing through the coil, we use the Faraday's Law of induction:

$$\varepsilon = -\frac{d\phi}{dt} \tag{A.1}$$

To calculate the total induced voltage, we add the induced voltage at each wire loop.

$$\varepsilon_{in} = -\sum_{k=1}^{N_r}\sum_{j=1}^{N_z} \frac{d}{dt}\phi(r_k, z_j, z_{mag}, \vec{B}_{mag}) \tag{A.2}$$

Magnetic flux ϕat each wire loop can be calculated as the double integral inside the loop of the dot product between the magnetic flux density produced by the magnet and the unitary vector $\hat{z}$, which means that only the vertical component will contribute to the variation of the magnetic flux.

$$\begin{aligned} \phi\left(z_{mag}, I, r_k, z_j\right) &= \int_0^{2\pi}\int_0^{r_k} \vec{B}_{mag}\cdot \hat{z}\, r dr\, d\theta \\ \phi\left(z_{mag}, I, r_k, z_j\right) &= \int_0^{2\pi}\int_0^{r_k} B_{mag}^{z} r dr\, d\theta \end{aligned} \tag{A.3}$$

The electric current trough the coil will induce a magnetic field that is opposed to the one produced by the magnet and its effect is modeled by means of the inductance of the coil, considered in the electric circuit.

An analytic expression to obtain the magnetic flux density in the vertical axis (Hawley, 2012) is:

$$B_{mag}^{z}(r, z_j, z_{mag}) = \frac{B_r R_{mag}}{4\pi} \int_{z_{mag}-\frac{h_{mag}}{2}}^{z_{mag}+\frac{h_{maag}}{2}} \int_{0}^{2\pi} \frac{\left(R_{mag} - r\cos(\psi)\right)}{\left(r^2 + R^2 + \left(z_j - \zeta\right)^2 - 2Rr\cos(\psi)\right)^{3/2}} d\psi d\zeta \qquad \text{(A.4)}$$

From this expression is seen that the value of the magnetic field in a point (r, z_j) depends on the magnet position relative to coil, the magnetic remanence (B_r) and of geometric parameters.

Replacing (A.3) in (A.2):

$$\begin{aligned}
\varepsilon_{in} &= -\sum_{k=1}^{N_r}\sum_{j=1}^{N_z} \frac{d}{dt}\int_0^{2\pi}\int_0^{r_k} B_{mag}^{z}(r, z_j, z_{mag}) r dr\, d\theta \\
\varepsilon_{in} &= -\sum_{k=1}^{N_r}\sum_{j=1}^{N_z} \int_0^{2\pi}\int_0^{r_k} \frac{dB_{mag}^{z}}{dz_{mag}}(r, z_j, z_{mag}) \frac{dz_{mag}}{dt} r dr\, d\theta \\
\varepsilon_{in} &= -\dot{z}_{mag}\sum_{k=1}^{N_r}\sum_{j=1}^{N_z} \int_0^{2\pi}\int_0^{r_k} \frac{dB_{mag}^{z}}{dz_{mag}}(r, z_j, z_{mag}) r dr\, d\theta \\
\varepsilon_{in} &= -\dot{z}_{mag} K_{\phi}(z_{mag})
\end{aligned} \qquad \text{(A.5)}$$

Next, the following change of variables $\bar{z} = \zeta - z_j \rightarrow d\bar{z} = d\zeta$ is applied (A.4) which gives:

$$B_{mag}^{z}(r, z_j, z_{mag}) = \frac{B_r R_{mag}}{4\pi} \int_{z_{mag}-\frac{h_{mag}}{2}-z_j}^{z_{mag}+\frac{h_{mag}}{2}-z_j} \int_{0}^{2\pi} \frac{\left(R_{mag} - r\cos(\psi)\right)}{\left(r^2 + {R_{mag}}^2 + \bar{z}^2 - 2R_{mag} r\cos(\psi)\right)^{\frac{3}{2}}} d\psi\, d\bar{z} \qquad \text{(A.6)}$$

The fundamental theorem of calculus stablishes that:

$$\frac{d}{dz}\int_{a(z)}^{b(z)} f(x)dx = f(b(z))\frac{db}{dz}(z) - f(a(z))\frac{da}{dz}(z) \qquad \text{(A.7)}$$

Then, considering (A.7) and deriving (A.6) with respect to time:

$$\frac{dB_{mag}^{z}}{dt} = \frac{dz_{mag}}{dt}\frac{dB_{mag}^{z}}{dz} = \dot{z}_{mag}\frac{dB_{mag}^{z}}{dz}\left(r, z_j, z_{mag}\right)$$

$$\frac{dB_{mag}^{z}}{dt} = \dot{z}_{mag}\frac{B_r R_{mag}}{4\pi}\left[\int_0^{2\pi}\frac{\left(R_{mag} - r\cos(\psi)\right)}{\left(r^2 + {R_{mag}}^2 + \left(z_{mag} + \frac{h_{mag}}{2} - z_j\right)^2 - 2R_{mag}r\cos(\psi)\right)^{\frac{3}{2}}}d\psi\right. \tag{A.8}$$

$$\left. - \int_0^{2\pi}\frac{\left(R_{mag} - r\cos(\psi)\right)}{\left(r^2 + {R_{mag}}^2 + \left(z_{mag} - \frac{h_{mag}}{2} - z_j\right)^2 - 2R_{mag}r\cos(\psi)\right)^{\frac{3}{2}}}d\psi\right]$$

Finally the expression for the electromagnetic coupling is:

$$K_\phi(z_0) = 2\pi\sum_{k=1}^{N_r}\sum_{j=1}^{N_z}\int_0^{r_k}\frac{B_r R_{mag}}{4\pi}\left[\int_0^{2\pi}\frac{\left(R_{mag} - r\cos(\psi)\right)}{\left(r^2 + R^2 + \left(z_{mag} + \frac{h_{mag}}{2} - z_j\right)^2 - 2R_{mag}r\cos(\psi)\right)^{\frac{3}{2}}}d\psi\right. \tag{A.9}$$

$$\left. - \int_0^{2\pi}\frac{\left(R_{mag} - r\cos(\psi)\right)}{\left(r^2 + {R_{mag}}^2 + \left(z_{mag} - \frac{h_{mag}}{2} - z_j\right)^2 - 2R_{mag}r\cos(\psi)\right)^{\frac{3}{2}}}d\psi\right] r dr$$

B. DERIVATION OF THE EQUATION OF MOTION

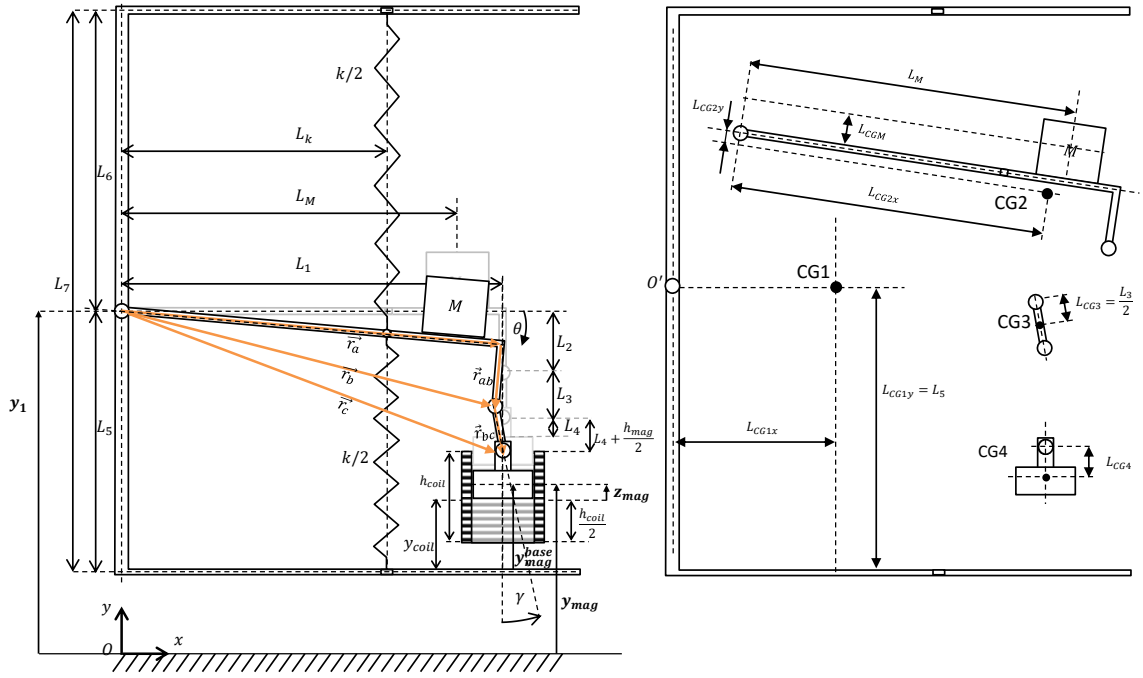

Using O as the origin the following relations are found:

$$\overrightarrow{r_{OO'}} = y_1\hat{\jmath}$$

$$\overrightarrow{r_a} = L_1\cos(\theta)\,\hat{\imath} - L_1\sin(\theta)\,\hat{\jmath}$$

$$\overrightarrow{r_{ab}} = -L_2\sin(\theta)\,\hat{\imath} - L_2\cos(\theta)\,\hat{\jmath}$$
$$\overrightarrow{r_{bc}} = L_3\sin(\gamma)\,\hat{\imath} - L_3\cos(\gamma)\,\hat{\jmath}$$
$$\overrightarrow{r_c} = \overrightarrow{r_a} + \overrightarrow{r_{ab}} + \overrightarrow{r_{bc}}$$

$$\overrightarrow{r_c} = [L_1\cos(\theta) - L_2\sin(\theta) + L_3\sin(\gamma)]\hat{\imath} + [-L_1\sin(\theta) - L_2\cos(\theta) - L_3\cos(\gamma)]\hat{\jmath}$$
$$\overrightarrow{r_c} = L_1\hat{\imath} - \left(y_1 - \left(y_{mag} + L_4 + \frac{h_{mag}}{2}\right)\right)\hat{\jmath}$$

$$\leftrightarrow L_1\cos(\theta) - L_2\sin(\theta) + L_3\sin(\gamma) = L_1$$
$$\leftrightarrow \sin(\gamma) = \frac{L_1}{L_3}(1 - \cos(\theta)) + \frac{L_2}{L_3}\sin(\theta)$$
$$\gamma = arcsin\left(\frac{L_1}{L_3}(1 - \cos(\theta)) + \frac{L_2}{L_3}\sin(\theta)\right)$$

$$-L_1\sin(\theta) - L_2\cos(\theta) - L_3\cos(\gamma) = -(y_1 - (y_{mag} + l_{CG4}))$$

$$L_1 \sin(\theta) + L_2 \cos(\theta) + L_3 \cos\left(arcsin\left(\frac{L_1}{L_3}(1 - \cos(\theta)) + \frac{L_2}{L_3}\sin(\theta)\right)\right) = (y_1 - \left(y_{mag} + L_4 + \frac{h_{mag}}{2}\right))$$

Now, using the relation $\cos(\arcsin(x)) = \sqrt{1 - x^2}$ gives:

$$L_1 \sin(\theta) + L_2 \cos(\theta) + L_3 \sqrt{1 - \left(\frac{L_1}{L_3}(1 - \cos(\theta)) + \frac{L_2}{L_3}\sin(\theta)\right)^2} = y_1 - \left(y_{mag} + L_4 + \frac{h_{mag}}{2}\right)$$

In order to reduce the expressions, the term $\sqrt{1 - \left(\frac{L_1}{L_3}(1 - \cos(\theta)) + \frac{L_2}{L_3}\sin(\theta)\right)^2}$ is approximated to 1. That approximation works fine for small angles and small values of L_2/L_3.

$$L_1 \sin(\theta) + L_2 \cos(\theta) + L_3 = y_1 - \left(y_{mag} + L_4 + \frac{h_{mag}}{2}\right)$$

Then an expression for the position (y_{mag}), velocity ($\dot{y}_{mag}$) and acceleration ($\ddot{y}_{mag}$) of the magnet in the vertical axis can be obtained as follows:

$$y_{mag} = y_1 - L_1 \sin(\theta) - L_2 \cos(\theta) - L_3 - L_4 - \frac{h_{iman}}{2}$$
$$\dot{y}_{mag} = \dot{y}_1 - L_1 \cos(\theta)\,\omega + L_2 \sin(\theta)\,\omega$$
$$\ddot{y}_{mag} = \ddot{y}_1 + L_1 sin(\theta)\omega^2 - L_1 cos(\theta)\alpha + L_2 cos(\theta)\omega^2 + L_2 sin(\theta)\alpha$$

In order to obtain the dynamic equations from Lagrange method, the kinetic and potential energy associated to each body must be calculated.

Body 1

$$K_1 = \frac{1}{2} M_1 \dot{y_1}^2$$
$$U_1 = M_1 g y_1$$

Body 2

Considering:

$$\hat{e}_r = \cos(\theta)\,\hat{\imath} - \sin(\theta)\,\hat{\jmath}$$

$$\hat{e}_\theta = \sin(\theta)\,\hat{\imath} + \cos(\theta)\,\hat{\jmath}$$
$$\frac{d\hat{e}_r}{dt} = -\sin(\theta)\,\dot{\theta}\hat{\imath} - \cos(\theta)\,\dot{\theta}\hat{\jmath} = -\hat{e}_\theta\dot{\theta} = -\hat{e}_\theta\omega$$
$$\frac{d\hat{e}_\theta}{dt} = \cos(\theta)\,\dot{\theta}\hat{\imath} - \sin(\theta)\,\dot{\theta}\hat{\jmath} = \hat{e}_r\dot{\theta} = \hat{e}_r\omega$$

The position of the center of mass is then:

$$\vec{r}_{CG2} = y_1\hat{\jmath} + l_{CG2x}\hat{e}_r - l_{CG2y}\hat{e}_\theta$$
$$= y_1\hat{\jmath} + l_{CG2x}(\cos(\theta)\,\hat{\imath} - \sin(\theta)\,\hat{\jmath}) - l_{CG2y}(\sin(\theta)\,\hat{\imath} + \cos(\theta)\,\hat{\jmath}\,)$$
$$= \big(l_{CG2x}\cos(\theta) - l_{CG2y}\sin(\theta)\big)\hat{\imath} + \big(y_1 - l_{CG2x}\sin(\theta) - l_{CG2y}\cos(\theta)\big)\hat{\jmath}$$

Thus the velocity is given by:

$$\vec{v}_{CG2} = \frac{d\vec{r}_{CG2}}{dt} = \dot{y}_1\hat{\jmath} - l_{CG2x}\omega\hat{e}_\theta - l_{CG2y}\omega\hat{e}_r$$
$$= \dot{y}_1\hat{\jmath} - l_{CG2x}\omega(\sin(\theta)\,\hat{\imath} + \cos(\theta)\,\hat{\jmath}) - l_{CG2y}\omega(\cos(\theta)\,\hat{\imath} - \sin(\theta)\,\hat{\jmath})$$
$$= \big(-l_{CG2x}\omega\sin(\theta) - l_{CG2y}\omega\cos(\theta)\big)\hat{\imath}$$
$$+ \big(\dot{y}_1 - l_{CG2x}\omega\cos(\theta) + l_{CG2y}\omega\sin(\theta)\big)\hat{\jmath}$$

$$\vec{v}_{CG2}{}^2 = v_{CG2x}^2 + v_{CG2y}^2$$
$$= \dot{y}_1 - 2\dot{y}_1 l_{CG2x}\omega\cos(\theta) + 2\dot{y}_1 l_{CG2y}\omega\sin(\theta) + l_{CG2x}^2\omega^2 + l_{CG2y}^2\omega^2$$

Finally, the kinetic energy and potential energy for body 2 is:

$$K_2 = \frac{1}{2}M_2\vec{v}_{CG2}{}^2 + \frac{1}{2}I_2\omega^2$$
$$U_2 = M_2 g\big(y_1 - l_{CG2x}\sin(\theta) - l_{CG2y}\cos(\theta)\big) + \frac{1}{2}\left(\frac{k}{2}\right)(L_6 - L_0 + L_k\sin(\theta))^2$$
$$+ \frac{1}{2}\left(\frac{k}{2}\right)(L_5 - L_0 - L_k\sin(\theta))^2$$

<u>Mass M</u>

$$\vec{r}_M = y_1\hat{\jmath} + L_M\hat{e}_r + l_{CGM}\hat{e}_\theta$$

The calculation for mass M is analog to body 2 (L_M *is to* l_{CG2x} *as* l_{CGM} *is to* $-l_{CG2y}$):

$$\vec{r}_M = (L_M\cos(\theta) + l_{CGM}\sin(\theta))\hat{\imath} + (y_1 - L_M\sin(\theta) + l_{CGM}\cos(\theta))\hat{\jmath}$$
$$\vec{v}_{CGM}{}^2 = \dot{y}_1 - 2\dot{y}_1 L_M\omega\cos(\theta) - 2\dot{y}_1 l_{CGM}\omega\sin(\theta) + L_M^2\omega^2 + l_{CGM}^2\omega^2$$

$$K_M = \frac{1}{2}M\vec{v}_{CGM}{}^2 + \frac{1}{2}I_M\omega^2$$
$$U_M = Mg(y_1 - L_M\sin(\theta) + l_{CGM}\cos(\theta))$$

<u>Body 3</u>

$$\vec{r}_{CG3} = y_1\hat{\jmath} + \vec{r}_b + \frac{\vec{r}_{bc}}{2}$$

$$\begin{aligned}\vec{r}_{CG3} &= y_1\hat{\jmath} + L_1\cos(\theta)\,\hat{\imath} - L_1\sin(\theta)\,\hat{\jmath} - L_2\sin(\theta)\,\hat{\imath} - L_2\cos(\theta)\,\hat{\jmath} + \frac{L_3}{2}\sin(\gamma)\,\hat{\imath} \\ &\quad - \frac{L_3}{2}\cos(\gamma)\,\hat{\jmath} \\ &= \left(L_1\cos(\theta) - L_2\sin(\theta) + \frac{L_3}{2}\sin(\gamma)\right)\hat{\imath} \\ &\quad + \left(y_1 - L_1\sin(\theta) - L_2\cos(\theta) - \frac{L_3}{2}\cos(\gamma)\right)\hat{\jmath}\end{aligned}$$

$$\begin{aligned}\vec{v}_{CG3} = \frac{d\vec{r}_{CG3}}{dt} &= v_{CG3x}\hat{\imath} + v_{CG3y}\hat{\jmath} \\ &= \left(-L_1\sin(\theta)\,\omega - L_2\cos(\theta)\,\omega + \frac{L_3}{2}\cos(\gamma)\,\dot{\gamma}\right)\hat{\imath} \\ &\quad + \left(\dot{y}_1 - L_1\cos(\theta)\omega + L_2\sin(\theta)\,\omega + \frac{L_3}{2}\sin(\gamma)\dot{\gamma}\right)\hat{\jmath}\end{aligned}$$

From past geometric relations:

$$\gamma = arcsin\left(\frac{L_1}{L_3}(1-\cos(\theta)) + \frac{L_2}{L_3}\sin(\theta)\right)$$

$$\dot{\gamma} = \frac{(L_1\sin(\theta) + L_2\cos(\theta))}{\sqrt{L_3^2 - (L_1(1-cos(\theta)) + L_2\,sin(\theta))^2}}\omega$$

$$\begin{aligned}\sin(\gamma) &= \sin\left(arcsin\left(\frac{L_1}{L_3}(1-cos(\theta)) + \frac{L_2}{L_3}sin(\theta)\right)\right) \\ &= \frac{L_1}{L_3}(1-cos(\theta)) + \frac{L_2}{L_3}sin(\theta)\end{aligned}$$

$$\begin{aligned}\cos(\gamma) &= \cos\left(arcsin\left(\frac{L_1}{L_3}(1-cos(\theta)) + \frac{L_2}{L_3}sin(\theta)\right)\right) \\ &= \frac{\sqrt{L_3^2 - (L_1(1-cos(\theta)) + L_2\,sin(\theta))^2}}{L_3}\end{aligned}$$

$$\cos(\gamma)\,\dot{\gamma} = \frac{(L_1\sin(\theta) + L_2\cos(\theta))}{L_3}\,\omega$$

$$\begin{aligned}\sin(\gamma)\,\dot{\gamma} &= \frac{(L_1\sin(\theta) + L_2\cos(\theta))}{L_3}\frac{(L_1(1-cos(\theta)) + L_2\,sin(\theta))}{\sqrt{L_3^2 - (L_1(1-cos(\theta)) + L_2\,sin(\theta))^2}}\omega \\ &\approx \frac{(L_1\sin(\theta) + L_2\cos(\theta))(L_1(1-cos(\theta)) + L_2\,sin(\theta))}{L_3^2}\,\omega\end{aligned}$$

$$\vec{v}_{CG3} = \frac{d\vec{r}_{CG3}}{dt} = v_{CG3x}\hat{\imath} + v_{CG3y}\hat{\jmath}$$
$$= \left(-L_1 \sin(\theta)\,\omega - L_2 \cos(\theta)\,\omega + \frac{(L_1 \sin(\theta) + L_2 \cos(\theta))}{2}\omega\right)\hat{\imath}$$
$$+ \left(\dot{y}_1 - L_1 \cos(\theta)\omega + L_2 \sin(\theta)\,\omega + \frac{1}{2}\frac{(L_1 \sin(\theta) + L_2 \cos(\theta))(L_1(1 - cos(\theta)) + L_2\, sin(\theta))}{L_3}\,\omega\right)\hat{\jmath}$$

$$\vec{v}_{CG3}^{\,2} = v_{CG3x}^2 + v_{CG3y}^2$$

The energy expressions add unnecessary complexity to the system, as the body 3 is the one with less energy of the system, so its contribution is neglected.

Body 4, Magnet

$$\vec{r}_{CG4} = L_1\hat{\imath} + y_{mag}\hat{\jmath}$$

$$= L_1\hat{\imath} + \left(y_1 - L_1 \sin(\theta) - L_2 \cos(\theta) - L_3 - L_4 - \frac{h_{mag}}{2}\right)\hat{\jmath}$$

$$\vec{v}_{CG4} = \frac{d\vec{r}_{CG4}}{dt} = (\dot{y}_1 - L_1 \cos(\theta)\,\omega + L_2 \sin(\theta)\,\omega)\hat{\jmath} = v_{CG4y}\hat{\jmath}$$

$$K_4 = \frac{1}{2}M_{mag}\vec{v}_{CG4}{}^2 = \frac{1}{2}M_{mag}v_{CG4y}^2$$
$$U_4 = M_{mag}g\left(y_1 - L_1 \sin(\theta) - L_2 \cos(\theta) - L_3 - L_4 - \frac{h_{mag}}{2}\right)$$

Generalized forces

The angle θ is chosen as a generalized coordinate in order to calculate the generalized force associated to the electromagnetic coupling:

$$Q_\theta = F_M(z_{mag})\frac{d\dot{y}_{mag}}{d\omega} = F_M(z_{mag})(-L_1 \cos(\theta) + L_2 \sin(\theta))$$

Where the position of the magnet relative to the coil z_{mag} is:

$$z_{mag} = y_{mag} - \left(y_1 - L_5 + \frac{h_{coil}}{2}\right)$$
$$= L_5 - L_1 \sin(\theta) - L_2 \cos(\theta) - L_3 - L_4 - \frac{h_{mag}}{2} - \frac{h_{coil}}{2}$$

$$\dot{z}_{mag} = \dot{y}_{mag} - \dot{y}_1 = -L_1 \cos(\theta)\, \omega + L_2 \sin(\theta)\, \omega$$

$$\ddot{z}_{mag} = \ddot{y}_{mag} - \ddot{y}_1 = L_1 sin(\theta)\omega^2 - L_1 cos(\theta)\alpha + L_2 cos(\theta)\omega^2 + L_2 sin(\theta)\alpha$$
$$\ddot{z}_{mag} = (L_1 \sin(\theta) + L_2 \cos(\theta))\omega^2 + (L_2 \sin(\theta) - L_1 \cos(\theta))\alpha$$

Friction

We assume that the system has friction loses associated to the viscous air friction of the magnet inside the coil and with the walls of the coil.

This friction term is considered as energy loses in the Lagrange formulation.

$$\Re = \frac{1}{2} C \dot{y}_{mag} = \frac{1}{2} C(-L_1 \cos(\theta)\, \omega + L_2 \sin(\theta)\, \omega)^2$$

$$\frac{\partial \Re}{\partial \dot{\theta}} = \frac{\partial \Re}{\partial \omega} = C(-L_1 \cos(\theta)\, \omega + L_2 \sin(\theta)\, \omega)(L_2 \sin(\theta) - L_1 \cos(\theta))$$

Lagrangian

$$L = K1 + K2 + KM + K4 - U1 - U2 - UM - U4$$

The dynamic equation is then obtained developing the Lagrange formulation given by:

$$Q_\theta = \frac{d}{dt}\left(\frac{\partial L}{\partial \dot{\theta}}\right) - \frac{\partial L}{\partial \theta} - \frac{\partial \Re}{\partial \dot{\theta}}$$

Using the symbolic algebraic software Maple, the development of the last expression is done but omitted due to its extension. The simplifications done were the following:

- Small angles : $\sin(\theta) = \theta$, $\cos(\theta) = 1$.
- Values of L_2, L_{CGM} and L_{CG2y} are neglected, then $L_2\theta = 0$.
- High order terms are null: $\theta^2 = 0,\ \theta^3 = 0,\ \theta^4 = 0$.
- $L_k^2 k - L_1^2 M_{mag} \omega^2 = L_k^2$.

C. DESIGN METHODOLOGY

The following design methodology allows the designer to choose a range of desired frequencies and a desired level of power. The inputs of the methodology are a given vibration obtained from measurements of the environment to be harvested and an initial configuration of the harvester, from which the algorithm will calculate the optimal coil and magnet, and the optimal values for ρ, l_k, σ & k .

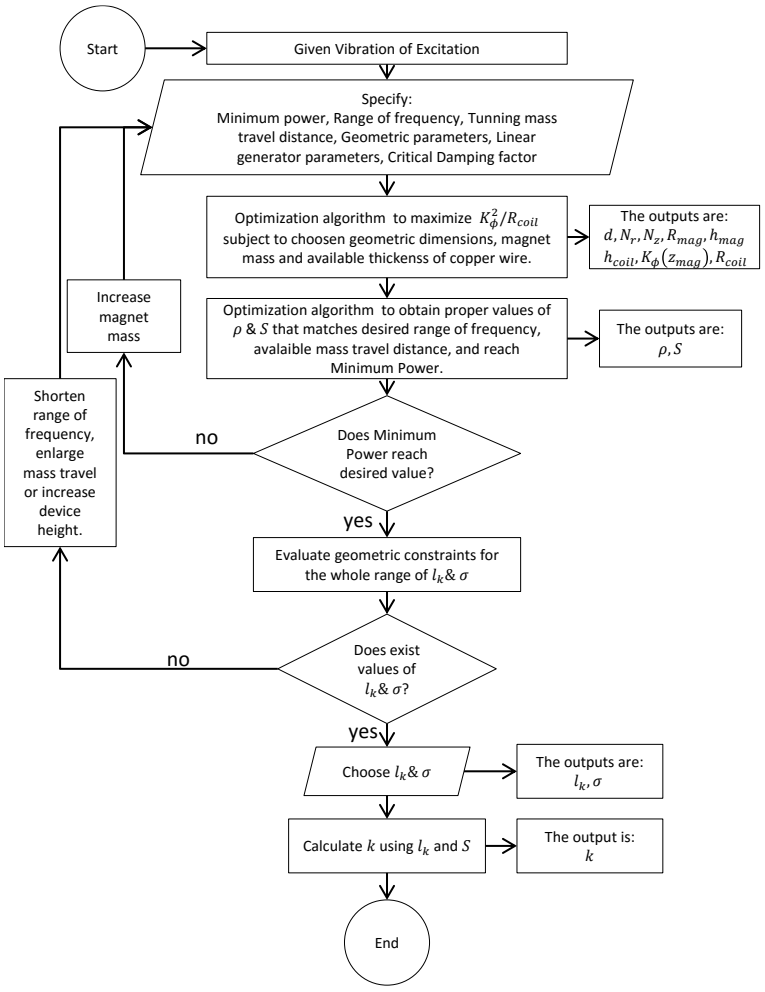

Figure C-1 Design Methodology

D. SIMILAR DEVICES FOUND IN LITERATURE

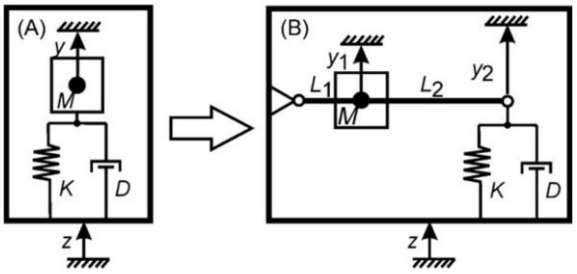

Fig. 1. Model of a conventional mass spring damper system (A) and of the mass spring damper system with lever mechanism to adjust its eigenfrequency (B).

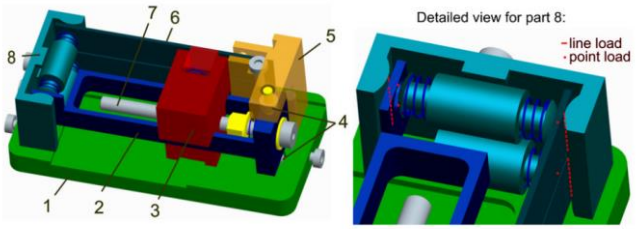

Figure D-1 From (Schaufuss & Mehner, 2012; Schaufuss et al., 2011).

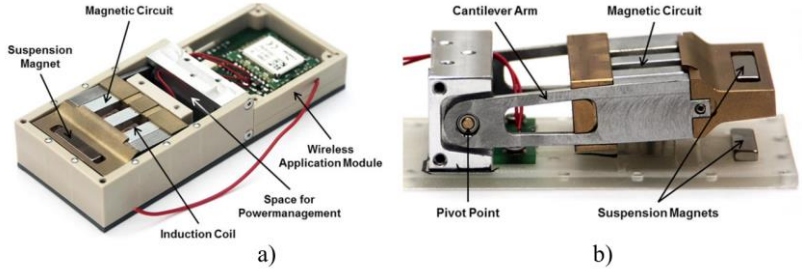

Figure 12. Implementation of the shock-excited energy harvester: (a) complete device (lid removed) including power management and wireless application module (b) side view showing the oscillating cantilever arm including magnetic circuit and suspension magnets.

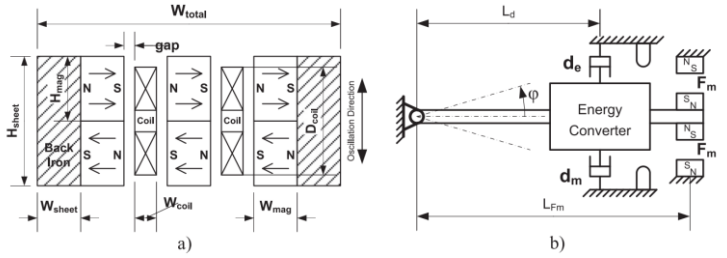

Figure 11. Shock-excited energy harvester: (a) schematic diagram (cross-section) of the active energy conversion structure showing the magnetic circuit and coils, (b) simplified model of the energy harvester including the nonlinear force F_m of the magnetic spring, mechanical stoppers and electrical and mechanical damping.

Figure D-2 From (Ylli et al., 2015)

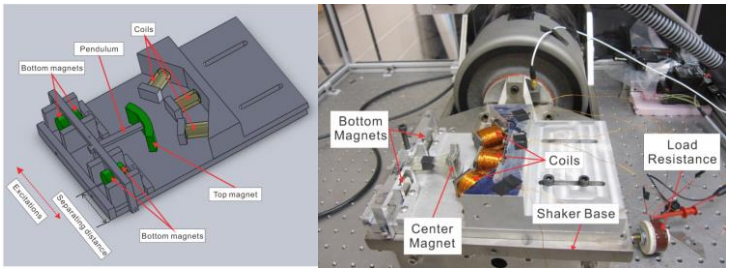

Figure D-3 From (X. Liu, 2012)

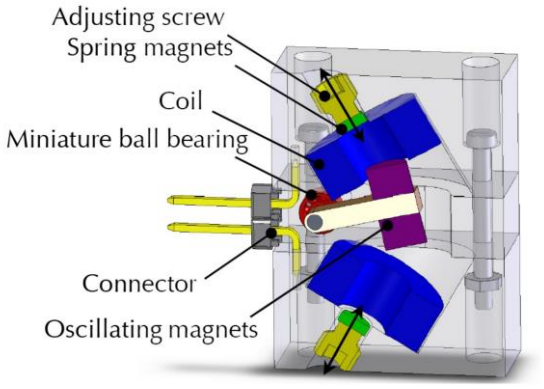

Figure D-4 From (Spreemann et al., 2006)

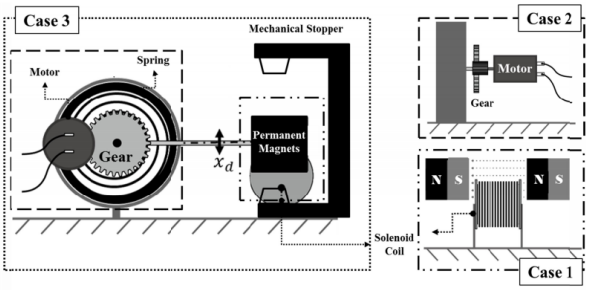

Figure 1. Schematic representation of the proposed energy harvesting device

Table 1. Three different device setups considered in this study

Cases	Contents
Case 1	Permanent magnets + Coil part
Case 2	Motor + Gear part
Case 3	Case 1 + Case 2 + Mechanical stopper

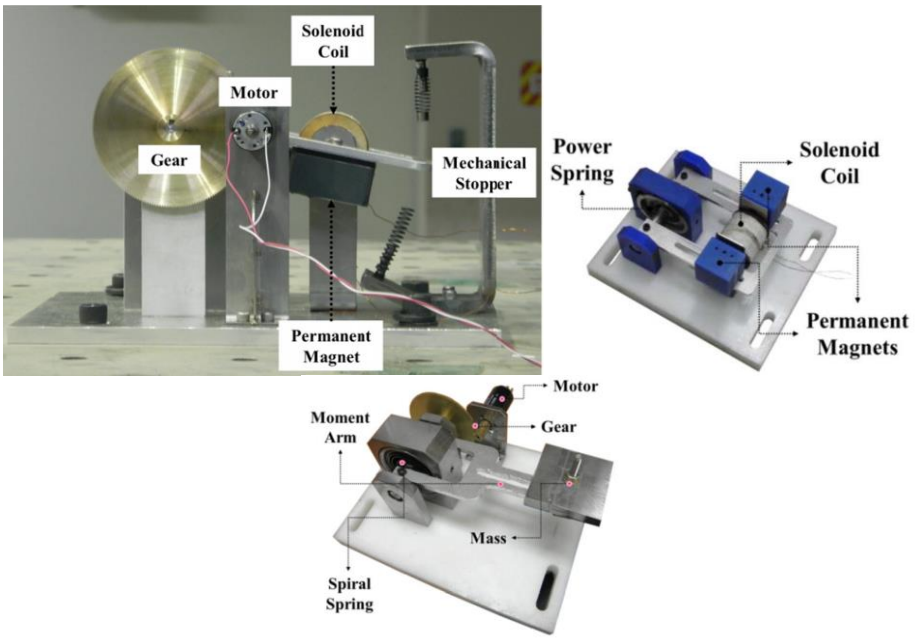

Figure D-5 From (H. J. Jung et al., 2012; H.-J. Jung et al., 2013; Kim et al., 2013)

E. PRELIMINARY PATENT SEARCH

N°	Patent ID	Title	Publication Date	Referencial drawing	Abstract
1	US 20120227485 A1	Balanced and Eccentric Mass Compact Pendulum with Dynamic Tuning	9/13/2012	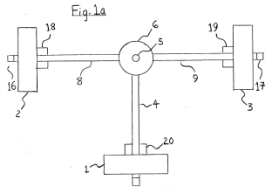	A pendulum combining balanced and eccentric masses oscillates with a period that is rapidly and continuously varied by shifting the balanced masses and eccentric mass to and from the rotational axis, by controlling the amplitude of oscillation and, in a rolling embodiment, by varying the curvature of the rolling surface. Long period oscillations can be achieved without the large heights required by an equivalent conventional pendulum. The pendulum can be substantively isochronous. The pendulum can be applied to harvesting vibrational energy and especially to wave energy extraction by dynamically achieving resonance over the typical frequency range of energetic ocean swell.
2	CN101359882A, CN101359882B	Resonance frequency adjustable piezoelectric vibration energy collecting device	8/17/2011	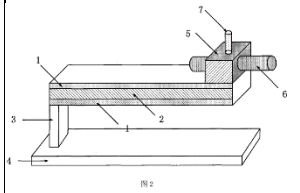	The invention discloses a resonance frequency adjustable piezoelectric vibration energy collecting device, which belongs to the energy conversion and the collection area of technology. The device to support the substrate as a vibration structure, by fixing the collected in the piezoelectric vibration energy. The device selected fixed mass and movable mass combined with the method, in a wide range of simply and accurately adjusting device the resonance frequency so as to maintain the ambient vibration mechanical resonance maximizing the vibration energy collecting capability. According to the invention realizes energy harvesting device, in large frequency range for the different vibration environment, and the sensor are combined, so that the sensor has self-powered capability.
3	WO 2006046937A1, CN100524870C, CN101002343A, EP1803170A1, EP1803170A4, EP1803170B1, US7471033, US20080129147,	Energy harvester with adjustable resonant frequency	5/4/2006	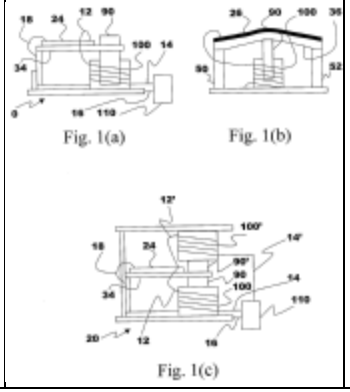	The present subject matter discloses devices, systems, and methodologies for harvesting power from environmentally induced vibrations. Piezoelectric devices (24) and structures are disclosed that may be employed in combination with electromagnetic (100) or capacitive (92, 94) elements to enhance the power harvesting capabilities of the piezoelectric devices (24). The electromagnetic (100) and capacitive (92, 94) elements may be used to assist in maintaining system mechanical resonance in order to maximize energy harvesting capabilities. Power harvesting devices and systems in accordance with the subject technology may concurrently operate as sensors in motion sensitive applications thus providing self-powered monitoring capabilities.

4	CN102392801A, WO2013060169A1	Gravitational energy conversion device and application thereof	9/25/2014	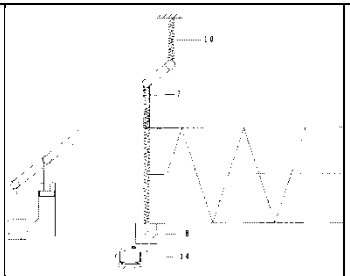	The invention discloses a gravitational energy conversion device, comprises a device frame, a weight, a luggage carrier, a combined spring, a chain, a ratchet wheels, a transmission shaft, flywheels, a limit latch, and a return spring. The transmission shaft is arranged on the device frame. The flywheels are arranged at both ends of the transmission shaft. The ratchet wheels are arranged on the transmission shaft. The ratchet wheels engage with the chain. One end of the chain is fixed to the limit latch, and the other end is connected to one end of the combined spring. Pairs of pawls which match the limit latch are arranged on inner sidewalls of the device frame in the same horizontal plane. One end of the return spring is fixed to the limit latch, and the other end is fixed to the luggage carrier.
5	EP1869755A1, CN101185230A, CN101185230B, US8080906, US20080278008, WO2006109033A1	Generator for converting mechanical vibrational energy into electrical energy	12/26/2007	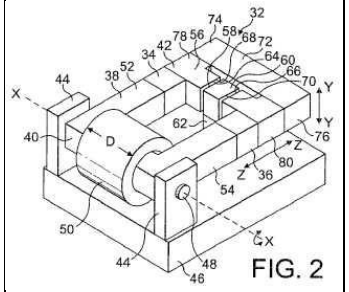 FIG. 2	An electromechanical generator (32) for converting mechanical vibrational energy into electrical energy, the electromechanical generator (32) comprising a substantially annular high-permeability core (38), the core (38) including at least one magnet (34, 36) therein to define a magnetic circuit, at least one rotatable bearing (48) mounting the core (38) to at least one bearing support (44), the at least one bearing (48) permitting the core (38) to pivot about a pivot axis (x-x), a gap (58, 68, 70) provided in the core (38), a body (60) of high-permeability material located in the gap (58, 68, 70), the body (60) being spaced from respective end faces (64, 66) of the core (38) by a respective spacing (58, 68, 70) whereby pivoting movement of the core (38) about the pivot axis (x-x) causes relative movement between the end faces (64, 66) of the core (38) and the body (60), and a rotationally fixed coil (50) surrounding a length of the core (60) coaxially with the pivot axis (x-x).
6	EP1869755A1, CN101185230A, CN101185230B, US8080906, US20080278088, WO2006109033A1	Adjustable viscoelastic vibration energy dissipator	9/17/1968	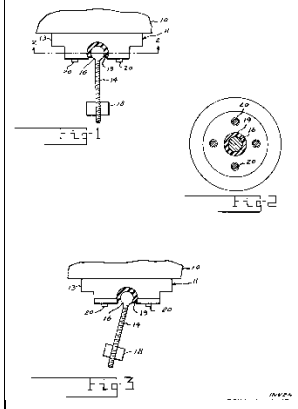	A shaft, having a ball on one end, has an inertial mass threadably supported thereon. A support body member adapted to be secured to the vibrating structure has a spherical cavity. A spherical shaped viscoelastic material having a spherical shaped cavity is secured in the cavity on the support body structure. The ball on the shaft is secured in the spherical shaped cavity in said viscoelastic material. In another embodiment, the inertial mass is supported on a wire attached to a pin supported by a viscoelastic material. An adjustable spring is attached t0 the other end of the pin

27	US7898157B2, US7692365, US7880370, US20070114890, US20100141096, US20100194240	Piezoelectric composite beam with automatically adjustable natural frequency	3/1/2011	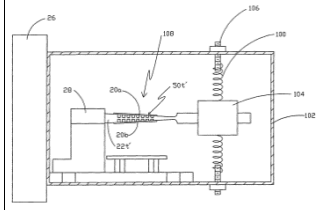	An energy harvesting system includes a composite structure that has a first spring, a piezoelectric structure, and a proof mass. The piezoelectric structure and the proof mass are mounted on the first spring. The composite structure has a natural frequency of vibration. The natural frequency of vibration of the composite structure is automatically adjustable.
7	US20140300113 A1, CN203840136U, WO2014162216A1	Energy harvester for converting vibrational motion of a vibrating equipment into electrical energy, and a device for monitoring the operation of a vibrating equipment	10/9/2014	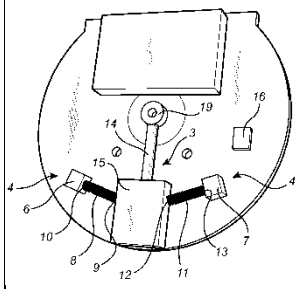	The invention relates to an energy harvester for converting vibrational motion of a vibrating equipment into electrical energy. The energy harvester comprises a pendulum arranged to be pivotably attached to said vibrating equipment, a motion limiter arranged to limit a pivoting motion of said pendulum, and a generator connected to said pendulum and arranged to convert said pivoting motion into electrical energy. The vibrational motion has an operating frequency, and said pendulum has a natural frequency different from said operating frequency. The invention also relates to a device for monitoring the operation of a vibrating equipment.
8	EP1869754, CN101204001A, CN101204001B, EP1869754A1, US8432084, US20100033142, WO2006109037A1	CONVERTING MECHANICAL VIBRATIONAL ENERGY INTO ELECTRICAL ENERGY	26/12/2007	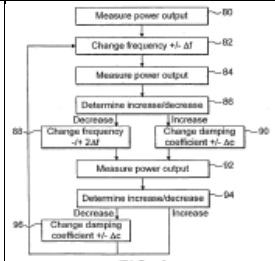 FIG. 6	An electromechanical generator comprising an electromechanical device for converting mechanical vibrational energy into electrical energy, the electromechanical device being a velocity damped resonator having a damping coefficient and a resonant frequency, a power detector for detecting the output electrical power from the electromechanical device, a controller, and a damping coefficient adjuster for adjusting the damping coefficient of the electromechanical device, the controller being arranged to control the damping coefficient adjuster in response to the output electrical power detected by the power detector.

F. XI CONCURSO DE PATENTAMIENTO VICERRECTORÍA DE INVESTIGACIÓN PONTIFICIA UNIVERSIDAD CATÓLICA DE CHILE

F.1 REVELACION DE LA INVECIÓN

Responsable de completar: El investigador

1. Título de la invención

Extractor de energía vibratoria tipo péndulo horizontal con frecuencia natural ajustable optimizado para vehículos pesados

2. Investigador y unidad académica responsable

(Indique: nombre, e-mail, anexo y facultad/escuela/instituto)

Benjamín Andrés Lagos Berríos, bálagos@uc.cl, Departamento de Ingeniería Mecánica Escuela de Ingeniería.

3. Inventores y otros participantes

Indique el nombre, Rut, profesión, cargo, email, dirección, anexo y unidad académica de los inventores, ya sea(n) investigador(es), estudiante(s), funcionario(s) o personal externo a la Universidad:

• **Luciano Chiang, 7029130-4, Profesor de Planta e Ingeniero (PhD), Jefe del Área, lchiang@ing.puc.cl, Los Orfebres 364-La Reina, DICTUC Mecatrónica.** • **Felipe Bravo, 15312806-5, Ingeniero Civil Industrial mención Ingeniería Eléctrica, Ingeniero de Proyectos, fabravov@uc.cl, Los Orfebres 364-La Reina, DICTUC Mecatrónica.**

4. Financiamiento de la invención y compromisos contraídos

Si la invención proviene del algún proyecto, por ejemplo FONDEF, INNOVA, indique:

Código de Proyecto	Fondo de Financiamiento
D10I1069	FONDEF

5. Descripción de la invención (producto o proceso) y problema que ésta resuelve

Describa las características de la invención que usted considera son "nuevas", los aspectos que la hacen única y no obvia, además de su aplicación industrial (como puede tener aplicación en la sociedad o el mercado).

En el marco del proyecto FONDEF N° D10I1069 se desarrollan e instalan sistemas adquisición y transmisión de datos, que apuntan a conseguir monitoreo continuo de la condición de operación de vehículos pesados.

Por la naturaleza de la actividad y el requerimiento de monitoreo continuo, el sistema de alimentación eléctrica de los módulos de monitoreo debe satisfacer las siguientes restricciones:

- La alimentación debe ser totalmente independiente del sistema eléctrico del vehículo estudiado, con tal de no interferir en su funcionamiento.
- Rápido de instalar y autónomo, por el restringido acceso a los vehículos cuando se encuentran en operación. Por esta razón, utilizar baterías se hace poco viable puesto que requieren reemplazo o recarga periódica.
- El sistema debe ser robusto, debido a las duras condiciones de operación a las que será sometido. Esto hace inviable la utilización de paneles solares.
- El consumo requerido por los módulos de monitoreo, para adquirir y transmitir las mediciones obtenidas de manera continua es del orden de 1W.

Las mediciones hechas demuestran la factibilidad de alimentar los sensores usando la energía proveniente de las vibraciones del vehículo producidas por la rugosidad del camino. La frecuencia de estas vibraciones varía según la velocidad del vehículo, entre otros parámetros.

Para cumplir con este objetivo se propone un sistema de extracción de energía vibratoria de bajas frecuencias (1-20Hz) que consiste en un péndulo horizontal en cuyo extremo se encuentra un imán que oscila en torno a una bobina, la cual produce un voltaje entre sus bornes.

La frecuencia natural del dispositivo se ajusta automáticamente con tal de alcanzar resonancia, lo que junto a la correcta elección de la carga eléctrica conectada y la posición de la bobina e imán usados, permiten extraer la máxima cantidad de energía posible. El ajuste de frecuencia se logra cambiando la posición de una masa en el péndulo usando un actuador lineal. La posición de equilibrio del imán con respecto a la bobina se ajusta usando un actuador lineal que mueve la bobina.

Además se desarrolló un modelo de la dinámica del dispositivo que permite obtener los parámetros de diseño necesarios para maximizar el rango de frecuencias en el que puede trabajar, simular su respuesta en el tiempo y probar distintas configuraciones con tal de adaptarse a los requerimientos de la aplicación para la cual se diseñará.

6. Ventajas de la invención

Indique cuál es la ventaja y/o diferencias de la invención en comparación con las alternativas existentes.

El sistema propuesto no interviene con la electrónica del vehículo a monitorear. Además no requiere recambio o recarga como ocurre con las baterías y se puede diseñar de manera de soportar duras condiciones de operación. Por su parte, el ajuste automático de frecuencia natural del generador y de la posición de la bobina lo adapta a vibraciones variables en el tiempo extrayendo la máxima cantidad de energía posible. Finalmente, el modelo dinámico desarrollado permite diseñar el sistema para distintas aplicaciones.

7. Estado de desarrollo de la invención

Describa el estado de desarrollo de la invención, incluyendo estado actual de la investigación:

PRUEBAS DE LABORATORIO		ENSAYOS IN VITRO	
PROTOTIPO	Sí	ENSAYOS IN VIVO	
PLANTA PILOTO			

Explicar otro: Se tiene un modelo validado del dispositivo y un prototipo de prueba de concepto funcional.

8. Firma del (los) inventor(es)

Mediante la firma de este documento, el(los) inventor(es) declara(n) conocer y aceptar la información entregada en el presente formulario.

Benjamín Andrés Lagos Berríos	_____	_____
Nombre del Inventor	Firma del Inventor	Fecha

F.2 SOLICITUD DE BÚSQUEDA DE ARTE PREVIO

Responsable de completar: El investigador

9. Título de la invención

Extractor de energía vibratoria tipo péndulo horizontal con frecuencia natural ajustable optimizado para vehículos pesados

10. Problema de la técnica que resuelve

Explique cómo la invención puede tener aplicación en la sociedad o el mercado.

El mantenimiento basado en la condición de operación para maquinaria pesada requiere de un sistema de monitoreo continuo que sea autónomo y robusto. Un punto crítico es la alimentación eléctrica de estos sistemas que debe satisfacer las siguientes restricciones:

- La alimentación debe ser totalmente independiente del sistema eléctrico del vehículo estudiado, con tal de no interferir en su funcionamiento.
- Rápido de instalar y autónomo, por el restringido acceso a los vehículos cuando se encuentran en operación. Por esta razón, utilizar baterías se hace poco viable puesto que requieren reemplazo o recarga periódica.
- El sistema debe ser robusto, debido a las duras condiciones de operación a las que será sometido. Esto hace inviable la utilización de paneles solares.
- El consumo requerido por los módulos de monitoreo, para adquirir y transmitir las mediciones obtenidas de manera continua es del orden de 1W.

La ventaja de esta aplicación es que existe una gran cantidad de energía vibratoria disponible que hace factible su extracción para alimentar sensores.
El dispositivo propuesto es capaz de trabajar en un amplio rango de frecuencias, variando su geometría para adaptar su frecuencia natural y sincronizarla con la frecuencia entrante con tal de entrar en resonancia. De esta manera puede extraer energía ante diferentes frecuencias de excitación, que para el caso de los vehículos pesados depende de sus características mecánicas (masa, rigidez y amortiguación), de la velocidad del vehículo y de las condiciones del terreno.

El monitoreo continuo de las condiciones de operación permite evitar fallas catastróficas de equipos de gran valor y ahorrar en costos de mantenimiento al alargar la vida útil de componentes.

Dadas sus características el sistema propuesto puede adaptarse a cualquier tipo de vehículo terrestre.

11. Estado de la técnica

Describa las soluciones existentes para el mismo o similar problema de la técnica. En el caso de tener conocimiento de patentes que solucionan parte del problema, identifíquelas.

1. Actualmente existen varios dispositivos en el mercado, por ejemplo:
ECO200, de Enocean: que convierte la energía usada para apretar un botón para enviar una señal de manera inalámbrica.
2. Vibration Energy Harvester (VEH), de Perpetuum: Dispositivo de tipo electromagnético tubular, diseñado para ciertas frecuencias fijas.

VEH-APA 400M-MD, de Cedrat-Technologies: dispositivo piezoeléctrico para 110Hz. Indican que es posible diseñar para una frecuencia dada por el comprador.

Volture PEH, de Mide: Dispositivos piezoeléctricos capaces de trabajar en amplios rangos de frecuencias 80Hz-170Hz o 60Hz-140Hz.

Por otro lado el mundo académico está trabajando constantemente en el desarrollo de sistemas de alimentación de Redes de Sensores Inalámbricos (RSI) usando la energía disponible en el medio ambiente.

En el artículo ***Zahid Kausar, a. S.M., Reza, A.W., Saleh, M.U. & Ramiah, H., (2014). Energizing wireless sensor networks by energy harvesting systems: Scopes, challenges and approaches.*** se trata el tema de la alimentación de RSI en general.

Energía solar, térmica y del movimiento son algunas de las fuentes usadas para alimentar RSI. En particular para las vibraciones las técnicas más usadas son basadas en piezoelectricidad, electrostáticos (capacitancia variable) y electromagnéticos.

El artículo ***Cepnik, C., Lausecker, R. & Wallrabe, U., (2013). Review on Electrodynamic Energy Harvesters—A Classification Approach. Micromachines, 4(2), 168–196.*** presenta una revisión de 67 conceptos de extractores de energía electromagnéticos que varían en rangos de 1Hz a 1kHz, aceleraciones entre 0.5 ms^{-2} y 100 ms^{-2} y tamaños de menos de 1cm^3 hasta más de 100 cm^3.

Si la aplicación tiene frecuencia de entrada variable, es deseable usar una técnica para modificar la frecuencia natural del dispositivo o bien ampliar su ancho de banda. En ***Zhu, D., Tudor, M.J. & Beeby, S.P., (2010). Strategies for increasing the operating frequency range of vibration energy harvesters: a review. Measurement Science and Technology, 21(2), 022001.*** se habla de las distintas técnicas posibles de usar. Realizar un ajuste de manera automática se puede hacer cambiando las características mecánicas del dispositivo o ajustando la carga eléctrica, ya sea de manera continua o intermitente. Este proceso conlleva un gasto de energía que debe ser evaluado de manera de no usar más de lo que se genera. Otra técnica corresponde al ampliar el ancho de banda usando arreglos de estructuras con diferentes frecuencias naturales, limitar la amplitud de oscilación, usar resortes no lineales, estructuras bi-estables o valerse de diferentes modos de vibración.

3. Dentro de los conceptos buscados, el más parecido sería el encontrado en ***J. Schaufuss, D. Scheibner, and J. Mehner, "New approach of frequency tuning for kinetic energy harvesters," Sensors Actuators A Phys., vol. 171, no. 2, pp. 352–360, Nov. 2011***, donde se plantea un dispositivo de péndulo horizontal de frecuencia natural ajustable con una masa en el brazo del péndulo. El ajuste es

manual y usa un sistema electrostático para extraer energía.

También se encontraron las siguientes patentes relacionadas identificadas por el código: US3401911 ; US20140300113 ; US20120227485 ; CN101359882B ; WO2006046937A1 ; US20140284938 ; EP1869755A1.

12. Variaciones de la invención

Indique variaciones y modificaciones que podrían resultar de la invención:

Aprovechando la configuración de péndulo se podría usar un generador rotatorio acoplado al sistema.
También se podría probar distintas maneras de modificar la rigidez, ya sea con placas metálicas delgadas, imanes opuestos, cuerdas elásticas, etc.

Otra modificación es probar distintas configuraciones de imanes y bobinas, por ejemplo usando imanes con magnetización en sentido radial con respecto al eje de rotación de la bobina.

13. Palabras claves

Indique las palabras claves más representativas para hacer la búsqueda del estado de la técnica:

Vibration Energy Harvesting, Electromagnetic Vibration Energy Harvester, Tunable Frequency Energy Harvester, Vibration Energy Scavenging, Vibration Operated Generator, Adaptive, Wideband, Energy Collector Scavenger, Vibration Absorber

14. Productos/procesos sustitutos

Describa los productos o procesos que podrían ser sustitutos a la invención.

Sistemas que alimenten a los sensores por medio de energía solar, calor o sacando energía magnética de cables de alta tensión o bien que reciban alimentación inalámbrica.

15. Patentabilidad de la invención

a. La presente invención tiene solicitud de patente vigente

SI	NO
	X

Título de la Patente	
Número o Código	
Fecha de presentación	
País donde se solicitó la patente	
Estudio Jurídico	

b. La invención ha sido presentada en algún evento y/o se han publicado documentos	SI	NO
		X

Eventos	
Publicaciones	

En caso afirmativo, o en el caso que se hubiera divulgado o publicado una materia estrechamente relacionada a la presente invención; favor completar en detalle en que se diferencia la presente invención de la materia ya presentada o publicada:

Máximo ½ página.		
c. Existen planes de presentación futura de la Invención en algún evento y/o de publicación de documentos	SI	NO
	X	

Eventos	
Publicaciones	

16. Firma de (los) inventor(es)

Mediante la firma de este documento, el(los) inventor(es) declara(n) conocer y aceptar la información entregada en el presente formulario.

Benjamín Andrés Lagos Berríos _____ _____

Nombre del Inventor Firma del Inventor Fecha

G. CONCLUSIONS OF THE STATE OF THE ART SEARCH

Clarke, Modet & Cº
CHILE

Huérfanos 835 piso 10
Edificio ópera
Santiago- Chile
Tel.: (56-2) 2433 68 30
Fax.: (56-2) 2433 68 31
info@clarkemodet.cl

IV CONCLUSIONES

La invención en estudio se relaciona con un dispositivo de extracción de energía a partir de vibraciones de baja frecuencias (1-20Hz) cuya configuración consiste en un péndulo horizontal en cuyo extremo se encuentra un imán que oscila en torno a una bobina, lo que produce un voltaje inducido entre sus bornes. El dispositivo permite ajustar la frecuencia natural cambiando la posición de una masa móvil en el péndulo usando un actuador lineal y manteniendo la posición de equilibrio del imán móvil con respecto a la bobina estática.

En la búsqueda del estado del arte previo, se encontraron varios documentos relacionados con dispositivo de extracción de energía a partir de vibraciones, el documento más cercano el documento 6 (WO2006046937A1), que describe al igual que la invención, un dispositivo de extracción de energía a partir de vibraciones cuya configuración consiste en un péndulo horizontal en cuyo extremo se encuentra un imán que oscila en torno a una bobina, este documento también considera una masa para ajustar la frecuencia del movimiento, siendo la principal diferencia, que no considera una disposición tipo balancín que le permita controlar la posición centralizada del imán con la bobina. Por lo tanto, la invención podría tener novedad y cumplir con el artículo 33 de la Ley.

Por otro lado, en cuanto al nivel inventivo, en otras palabras, que se deriven de manera evidente de la combinación de los documentos encontrados u obvios a los ojos de un experto de la materia, el documento 6 no presenta un movimiento tipo balancín ni un sistema de control de masa que permita mantener centralizada la bovina con el imán, el documento 5 en cambio, si considera un movimiento tipo balancín, pero este documento está pensado para otro tipo de movimientos y no para centralizar el imán con la bobina, por lo tanto, la invención podría tener nivel inventivo, pero debe demostrar un

Huérfanos 835 piso 10
Edificio ópera
Santiago- Chile
Tel.: (56-2) 2433 68 30
Fax.: (56-2) 2433 68 31
info@clarkemodet.cl

beneficio no esperado al utilizar este tipo de configuración a diferencia de las encontradas en el estado del arte.

De acuerdo con el artículo 36 de la Ley, se considera que una invención es susceptible de aplicación industrial cuando su objeto pueda, en principio, ser producido o utilizado en cualquier tipo de industria, por lo tanto, concluimos que esta invención tendría aplicación en la industria y esta, de ser mencionada explícitamente en una posible redacción de solicitud de patente, daría cumplimiento con la Ley.